

PALACKÝ UNIVERSITY OLOMOUČ

FACULTY OF SCIENCE

DEPARTMENT OF PHYSICAL CHEMISTRY

**Modelling of graphene derivatives and their
interactions**

Master's thesis

Author: Bc. Martin Vondrák

Supervisor: Mgr. Martin Pykal, Ph.D.

Subject of study: Physical Chemistry

OLOMOUČ 2021

Declaration

I declare that I elaborated my master's thesis independently under the supervision of
Mgr. Martin Pykal, Ph.D., and all sources are included in the bibliography.

In Olomouc, date:

.....

Martin Vondrák

Acknowledgment

I cannot express enough thanks to my supervisor Mgr. Martin Pykal, Ph.D. for his leadership, valuable advice, and patience with me.

A huge acknowledgment goes to my family and friends, who supported me and kept my sanity in one piece and reminded me that leaving the house every once in a while is a good thing.

Bibliographical identification:

| | |
|-------------------------|---|
| Author: | Martin Vondrák |
| Title: | Modelling of graphene derivatives and their interactions |
| Type of thesis: | Master's |
| Department: | Department of Physical Chemistry |
| Supervisor: | Mgr. Martin Pykal, Ph.D. |
| The year of submission: | 2021 |
| Abstract: | <p>Reactions known from organic chemistry are not generally transferable to 2D materials. Their topology contains a large number of uncertainties arising from the used precursor, production method, and many others. Moreover, the simple mechanical accessibility of the grafted group, where the chemistry takes place, may be considerably limited by the spacious surface. Cyanographene is one of the newest graphene derivatives with 15 % of its surface covered by nitrile groups. Similarly to its aliphatic counterparts, cyanographene can undergo a hydrolysis reaction, which leads to graphene acid. Although aliphatic nitrile molecules can be reduced, the reaction of cyanographene with LiAlH_4 as the reducing agent is ambiguous. For this reason, this work studied the mechanistic part of the cyanographene reduction in tetrahydrofuran by classical molecular dynamics simulations. First, graphene-induced layering of the tetrahydrofuran molecules was observed, which acted as a barrier between the reducing agent and functional group. Moreover, different approach directions of the reducing agent to the functional group on cyanographene and aliphatic molecules were observed, based on the topology of the surface and the aliphatic chain. These access directions together with limited group accessibility can explain, why the reduction of cyanographene is not favorable in comparison to its aliphatic counterparts.</p> |
| Keywords: | graphene, cyanographene, accessibility, molecular mechanics |
| Number of pages: | 70 |
| Language: | English |

Bibliografická identifikace:

| | |
|----------------------|--|
| Autor: | Martin Vondrák |
| Název: | Modelování grafenových derivátů a jejich interakcí |
| Typ práce: | Diplomová |
| Pracoviště: | Katedra fyzikální chemie |
| Vedoucí: | Mgr. Martin Pykal, Ph.D. |
| Rok odevzdání práce: | 2021 |
| Abstrakt: | <p>Reakce známé z organické chemie obecně nejsou použitelné v chemii 2D materiálů. Finální topologie 2D struktur závisí na použitém prekursoru, metodě přípravy apod. Navíc jednoduchá mechanická přístupnost funkčních skupin pro chemická činidla může být výrazně omezena samotným povrchem 2D materiálu. Jedním z nejnověji objevených derivátů grafenu je kyanografen. Jeho povrch je pokryt z 15 % nitril skupinami, které se standardně vyskytují v organické syntéze. Analogicky k jeho alifatickým protějškům bylo ukázáno, že kyanografen může být kysele hydrolyzován na grafenovou kyselinu. Na druhou stranu úspěšná redukce kyanografenu pomocí LiAlH_4 je nejasná, a proto se tato práce zabývala studiem mechanické části této reakce. Za tímto účelem byly použity metody molekulové mechaniky, které umožnily porovnat přístup mezi alifatickými molekulami a kyanografenem v tetrahydrofuranu. Simulace ukázaly silné strukturování tetrahydrofuranu na povrchu grafenu, které tvořilo bariéru mezi LiAlH_4 a funkční skupinou. Zároveň simulace s alifatickými molekulami demonstrovaly, že redukující činidlo může přicházet k funkční skupině z odlišných směrů v závislosti na topologii alifatického řetězce. Tento přístup nelze aplikovat na kyanografenu, jelikož jeho reakční prostor je striktně omezen. Toto samotné sterické bránění 2D povrchu může napovědět, proč redukce kyanografenu zatím nebyla úspěšně provedena.</p> |
| Klíčová slova: | grafen, kyanografen, přístupnost, molekulová mechanika |
| Počet stránek: | 70 |
| Jazyk: | Angličtina |

Contents

| | | |
|----------|--|-----------|
| 1 | Introduction | 8 |
| 2 | Two-dimensional materials | 10 |
| 2.1 | Graphene | 10 |
| 2.1.1 | Graphene preparation | 12 |
| 2.2 | Graphene derivatives | 15 |
| 2.2.1 | Graphane | 16 |
| 2.2.2 | Graphene oxide | 16 |
| 2.2.3 | Fluorographene | 17 |
| 2.2.4 | Cyanographene | 18 |
| 2.2.5 | Graphene acid | 19 |
| 2.3 | Reactivity of graphene derivatives | 20 |
| 2.3.1 | Graphene oxide | 20 |
| 2.3.2 | Fluorographene | 21 |
| 3 | Methods | 24 |
| 3.1 | Computational chemistry | 24 |
| 3.2 | Molecular mechanics | 25 |
| 3.2.1 | Covalent terms | 26 |
| 3.2.2 | Non-covalent terms | 28 |
| 3.3 | Molecular dynamics | 31 |
| 4 | Reduction of cyanographene | 34 |
| 4.1 | Mechanism of the reduction | 35 |
| 4.2 | Simulations description | 36 |
| 4.3 | Results and discussion | 38 |
| 4.3.1 | Differences in solvents | 39 |
| 4.3.2 | Graphene-induced THF structuring | 40 |

| | | |
|----------|---|-----------|
| 4.4 | Molecular accessibility of nitriles | 42 |
| 4.4.1 | Access directions | 49 |
| 5 | Summary | 54 |
| 6 | Závěr | 55 |
| | Bibliography | 56 |
| | Supplementary Material | 68 |

List of Abbreviations

| | |
|------|------------------------------------|
| 2D | two-dimensional |
| HOPG | highly oriented pyrolytic graphite |
| CVD | chemical vapor deposition |
| EPR | electron paramagnetic resonance |
| NMR | nuclear magnetic resonance |
| NMP | <i>N</i> -methylpyrrolidon |
| DMA | <i>N,N</i> -dimethylacetamide |
| DMEU | 1,3-dimethyl-2-imidazolidinone |
| THF | tetrahydrofuran |
| DMF | <i>N,N</i> -dimethylformamide |
| GO | graphene oxide |
| rGO | reduced graphene oxide |
| FG | fluorographene |
| GCN | cyanographene |
| QM | quantum mechanics |
| DFT | density functional theory |
| WFT | wave function theory |
| HF | Hartree-Fock method |
| MM | molecular mechanics |
| FF | force field |
| vdW | van der Waals |
| MD | molecular dynamics |
| PBC | periodic boundary condition |
| RDF | radial distribution function |
| LJ | Lennard-Jones |
| EPS | electrostatic potential |
| REPS | restrained electrostatic potential |
| SPC | simple point charge |

1. Introduction

2004 was the breakthrough year for material scientists because the first two-dimensional material - graphene - was prepared. After its discovery, it was found that graphene has exceptional mechanical, electrical, and optical properties, some of which were not found in any other material. Thanks to that, graphene can be potential applied in many different fields. Nevertheless, some graphene characteristics limit its applicability in technologies as semiconductors or biomedicine technology. Fortunately, these limitations can be overcome by chemical modifications of graphene. These reactions were mainly performed with graphene oxide as the precursor for further graphene functionalization. However, graphene oxide topology is hard to reproduce and strongly depends on the preparation methods.

On the contrary, fluorographene discovery initiated a boom in graphene chemistry. Despite the expected chemical inertness, fluorographene can participate in various reactions. Soon, it was demonstrated that fluorographene can undergo reductive defluorination, or nucleophilic substitution reactions. Fluorographene can react with amines or alcohols, which creates new covalent functionalized graphene derivatives, by substituting some fluorine atoms. On the other hand, sulfur nucleophiles act more as reducing agents. Moreover, alkylation and arylation of graphene were performed by well-known Grignard reactions with fluorographene. Furthermore, fluorographene can be modified via reactions with inorganic substances, as are hydrosulfides, hydroxide ions, and pseudohalides.

The ability of cyanide to substitute fluorine atoms of fluorographene allowed the preparation of cyanographene. It is a non-stoichiometric derivative, which has 15 % of its surface covered by nitrile groups. Consequently, this derivative can undergo some reactions known from its organic counterparts. For example, acid hydrolysis led to the preparation of graphene acid. However, although organic nitrile can be reduced to amines by the strong reducing agent, the reduction of cyanographene is still missing in impacted literature. For this reason, I decided to study the mechanistic part of the cyanographene reduction with classical molecular dynamic simulations.

The following text will introduce graphene and series of its derivatives and their chemistry, followed by a basic introduction to molecular mechanics, which allows computing large systems containing thousands of atoms. The second part of this thesis will be focused on the accessibility of LiAlH_4 to cyanographene and organic functional group of nitrile molecules in the tetrahydrofuran.

2. Two-dimensional materials

A material that can be classified as two-dimensional (2D) has to have one dimension below 100 nm. [1] Although many 2D materials are under development, this work is focused solely on graphene and its closest derivatives.

2.1 Graphene

Graphene can be considered as a revolutionary material. Its discovery in 2004 made by scientists Andrew Geim and Konstantin Novoselov started a new era in material science. [2] Soon after, both scientists were awarded the Nobel Prize in physics for „groundbreaking experiments regarding the two-dimensional material graphene“. The significance of the discovery was supported by the premise (generally accepted before 2004) that two-dimensional materials are not thermodynamically stable, because thermal fluctuations of atoms would cause a deviation in the lattice comparable with interatomic distances in graphene (or any 2D material), which would decompose into smaller fragments at any temperatures. Thus, graphene was considered as a theoretical and computational model only. [3] The unexpected stability of the 2D crystal was partly explained by a wrinkled lattice (i.e., the sheet is not perfectly flat, as can be seen in Figure 1). [4] However, a number of other 2D materials have been discovered since the first graphene preparation. [5]

Graphene is an allotrope of carbon. Carbon atoms are organized into a one atom thick honeycomb-like flat structure. Each non-edge carbon atom of graphene is sp^2 hybridized and covalently bonded to 3 neighboring atoms. The length of C–C σ bonds is approximately 0.142 nm. [6] Thanks to these strong σ bonds, graphene has a high Young’s modulus $E = 1 \text{ TPa}$ and the value of its breaking strength is 42 N m^{-2} , [7] which is $100\times$ higher compared to the value of steel. It should be noted that these values can be applied to pristine graphene only because imperfections, which are incorporated in the graphene structure, decrease graphene stress resistance. [8] Moreover, graphene has one of the biggest surface areas reaching to $2630 \text{ m}^2 \text{ g}^{-1}$, which is a sufficient value to cover a football field just by one

gram of graphene. [9]

The graphene structure is surrounded by two π -electron clouds formed by the interaction of the fourth unhybridized carbon p orbitals, which are perpendicular to the lattice. The clouds of electrons give graphene its aromatic character and intriguing electronic features. Because the valence and conduction bands meet at the Dirac point, graphene is considered a semiconductor with a zero band gap. [10] The velocity of electrons may reach up to 10^6 m s^{-1} , which is due to little restrictions in their movement. However, defects in the lattice of the crystal act as scattering sites, which inhibit charge transport, and therefore a mean free path of electrons is lowered. [11] Furthermore, delocalized electrons can be described as *Dirac fermions*, which means they can behave as massless relativistic particles. [11, 12] These properties cause graphene high electron mobility of $100\,000$ $\text{cm}^2 \text{V}^{-1} \text{s}^{-1}$ with a theoretical limit up to $200\,000$ $\text{cm}^2 \text{V}^{-1} \text{s}^{-1}$. [13, 14]

Besides its excellent electric conductivity, graphene is also an exceptional thermal conductor. The value of the thermal conductivity was measured to be around $5\,000$ $\text{W m}^{-1} \text{K}^{-1}$ at a room temperature, [15] which exceeds the thermal conductivity of copper and other carbon allotropes as diamond or graphite. [16] However, if graphene is placed on the substrate, the thermal conductivity decreases. For instance, graphene on SiO_2 or Cu displays the thermal conductivity only 600 $\text{W m}^{-1} \text{K}^{-1}$ [16] and 370 $\text{W m}^{-1} \text{K}^{-1}$ [17], respectively. The lower thermal conductivity of the supported graphene is probably caused by a strong scattering and leaking of phonons across the substrate-graphene interface. [18]

Optical properties of bulk graphene and graphite can be observed with simple pencil drawings. The graphene color varies from gray to black, depending on the number of layers. Similarly, it can be also observed in the dispersion of graphene in the organic solvents. This shows graphene ability to absorb white light. A single graphene layer transmits 96.7 % of the white light, whereas the transmittance of five graphene layers decreases to 88 %. Thus each layer of graphene decreases transmittance by 2.3 %. Moreover, graphene reflects only 0.1 % of the incident light. [19]

Finally, the main difference from its 3D counterpart - graphite - is based on the electronic structure. The semi-metal characteristics of graphene are changing with an increasing number of the layers, as the valence and conduction bands start to overlap. The band overlap is 1.6 meV in the two-layer graphene. With more than 11 layers, one starts to talk about

graphite because the difference from the bulk electronic structure is just 10 % with the bands overlap of 41 meV. [20]

In the view of the above-mentioned unique properties, graphene can be used in various fields, e.g., energy storage (material in batteries [21, 22] or electrode materials for the supercapacitors [23, 24]), biosensing [25], or photonics and optoelectronics [26].

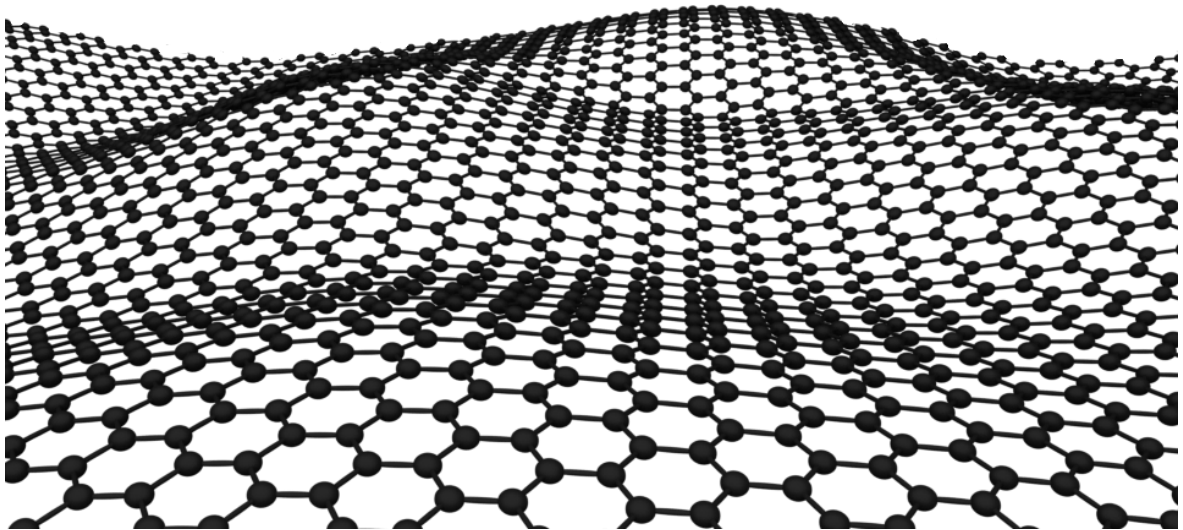


Figure 1: Graphene structure showing surface undulations.

2.1.1 Graphene preparation

Preparation methods of graphene (and 2D nanomaterials in general) can be divided into two main branches (Figure 2). First are *top-down* methods, which are based on the size reduction of relatively large materials into smaller particles. On the other hand, *bottom-up* methods build nanoparticles from individual molecules or atoms. [27]

Top-down methods

Graphene was firstly prepared by *mechanical exfoliation* in 2004. The method is sometimes called *scotch-tape technique* because it can be performed by peeling carbon layers from highly oriented pyrolytic graphite (HOPG) with the use of a classic scotch-tape. By using the scotch-tape method, a large-high-quality crystal of graphene can be produced. [28]

Mechanical exfoliation is used mainly to produce graphene for proof of concept devices such as graphene transistors [29], or state-of-the-art sensors of gases with a single-molecule sensitivity [30]. Despite the possibility of creating large graphene flakes, the method is time-consuming, and therefore it is not suitable for mass production.

A liquid phase exfoliation of graphite can be utilized for the preparation of a larger amount of graphene. A graphite suspension is dispersed in a suitable solvent, followed by ultrasonication, which creates a colloid solution of individual graphene layers. The energy needed for the separation of layers is compensated by the solvent-graphene interaction. Therefore the most important property of the chosen solvent is its surface energy. [31] In practice, different solvents are considered, for instance perfluorinated aromatic solvents [32], N-methylpyrrolidone (NMP), N,N-dimethylacetamide (DMA), and 1,3-dimethyl-2-imidazolidinone (DMEU) [31]. Moreover, surfactant additives can be used if the graphene aqueous dispersion is needed. [33]

Both mentioned procedures are using pure carbon as a source. However, graphene can be also produced by the *reduction of graphene oxide (GO)*. GO can be reduced to *reduced graphene oxide (rGO)* by heating GO in the quartz tube with an Ar atmosphere [34], or chemically (for example, by using hydrazine N_2H_4 [35] or sodium borohydride $NaBH_4$ [36]). It is worth noting that this process is very complex and difficult, and various oxygen groups and numerous defects are always present in the structure of final graphene after the reduction. [37]

Bottom-up methods

Epitaxial growth on a crystalline silicon carbide (SiC) surface is a promising way to prepare high-quality graphene on a large scale. SiC has more than 200 modifications, but only three of them are relevant for graphene production: 3C-, 4H- and 6H-SiC. Thermal annealing (around 1500 K) under high vacuum causes sublimation of silicon atoms from the SiC crystal and leaves a carbon-rich layer on the surface. Graphene can be made from both sides, silicon-rich, and carbon-rich, but the final product is different on each side. If the C-rich side is used, graphene is rapidly formed and creates a thick multilayer film. On the other hand, the Si-rich side produces a thin layer of graphene. Various graphenes with different structures, properties, or heteroatom dopants can be prepared due to the wide range of possi-

ble modifications of this method. The epitaxial growth of graphene can also be done by the decomposition of carbon-containing molecules by heating them while using a metal surface as a catalyst, or by thermal segregation of carbon atoms in carbon-rich metals. [38, 39]

During the epitaxial growth, the source of carbon is the structure of the annealed material itself. In contrast, *chemical vapor deposition* method (CVD) uses an external source of carbon. Generally speaking, a gas containing carbon is deposited on the metal surface under low pressure and high temperature. Prepared graphene can be then transferred to another substrate. The most used substrates are nickel, copper, and cobalt. Copper is suitable for the production of the graphene monolayer, and nickel is usually used for the controlled preparation of multilayer graphene. Next to Cu and Ni, some other metals were investigated as possible candidates for substrates; iron, ruthenium, palladium, and even stainless steel. Commonly used gaseous sources of carbon are methane or ethylene. Furthermore, the addition of other components to the mixture can be used to control the quality and properties of final graphene. Adding hydrogen to the mixture allows growing large single-layer graphene. The addition of oxygen to the mixture is equally important because it can passivate the surface of the metal. As a result of the passivation, graphene nucleation density is lowered, which creates larger size graphene flakes. [40]

Besides the introduced methods, some less frequently used preparations are in development. The preparation of the graphene nanoribbons by *carbon nanotubes unzipping* is one of them. High-yield unzipping can be achieved by the reaction of potassium permanganate with multi-walled nanotubes. Along with the chemical route, the argon plasma etching of nanotubes can create precisely defined graphene nanoribbons. [41] Finally, *total synthesis* can be used for the preparation of nanographene. Reactions as Suzuki coupling or intramolecular oxidative cyclodehydrogenations can be applied. [42]

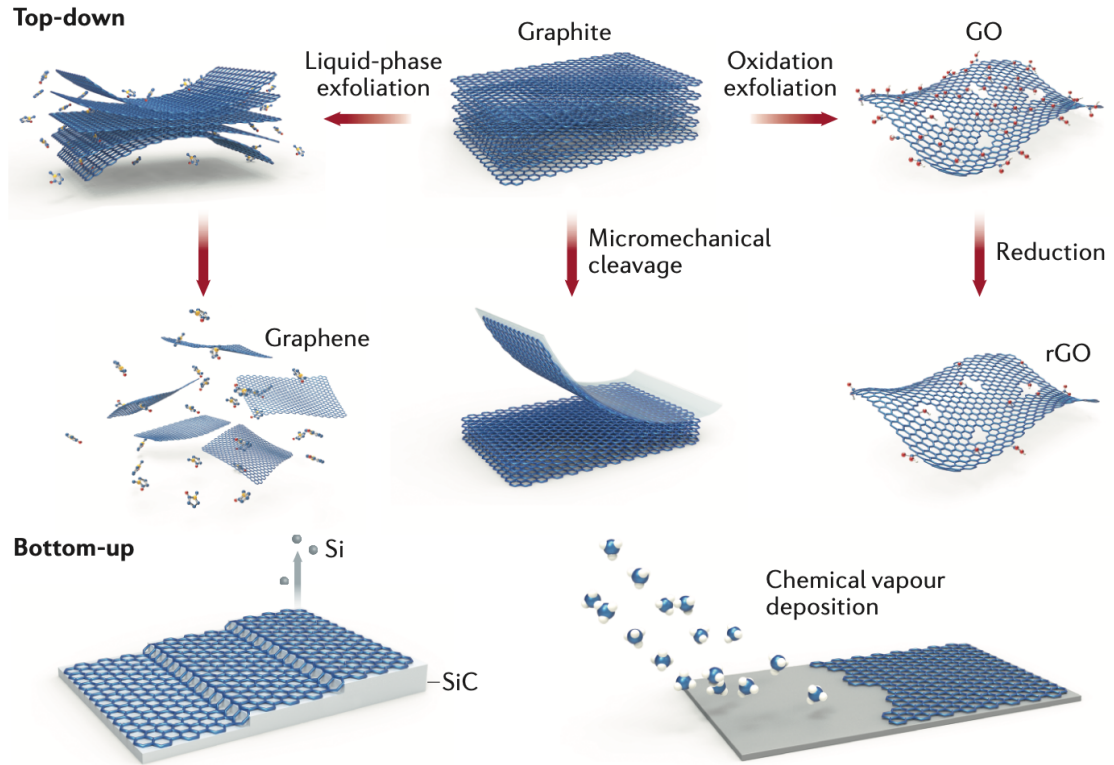


Figure 2: Schema of various graphene preparations. [43]

2.2 Graphene derivatives

Despite superior graphene properties, not all of them are suitable for some specific applications. For example, the zero band gap limits the graphene usage in semiconductor technologies, graphene hydrophobicity is unwanted in some bioapplications, or its relative chemical inertness represents a problem with a further graphene functionalization. [44, 45, 46] Material physicists and chemists around the world have been focused on graphene modification in the past years to overcome these limitations.

The graphene reactivity is similar to the reactivity of polyaromatic hydrocarbons, so it can undergo various reactions that are well-known from organic chemistry. Only derivatives based on the formation of bonds between functional groups and sp^3 hybridized graphene carbons will be discussed in more detail in this work. Although the covalent graphene functionalization can be done by incorporating heteroatoms (mainly boron, nitrogen, or sulfur) into a carbon lattice, these modifications are out of the scope of this thesis and therefore they will not be described in the following text. [47, 48, 49]

2.2.1 Graphane

Fully hydrogenated graphene - *graphane* - is a stoichiometric graphene derivative. Alternatively, graphene that is not fully hydrogenated is called *hydrogenated graphene* rather than graphane. [50] The first graphane synthesis was performed by a reaction of pristine graphene with a cold hydrogen plasma. [51] Furthermore, graphane can be produced by Birch reduction, where an alkali metal serves as a reducing agent in liquid ammonia or in tetrahydrofuran (THF) with a water or alcohol addition. [52] Due to the reversibility of graphane hydrogenation through its annealing, the derivative is considered as a promising hydrogen storage material. [50, 51]

2.2.2 Graphene oxide

In contrast to graphane, graphene oxide is a non-stoichiometric derivative of graphene. Furthermore, GO could be considered as a group of compounds rather than one particular structure due to the randomly distributed oxygen-containing chemical groups on its surface. In the generally accepted model, the hydroxyl and epoxy groups are mostly on the basal plane, while edges can contain carboxyl, carbonyl, phenol, lactone, or quinone groups. One of the possible chemical structures of GO is shown in Figure 3. The sp^3 carbons in the lattice of graphene oxide cause a planarity disruption. Thus, the final topology of the graphene oxide strongly depends on the used synthesis method. [53, 54] In comparison to graphene, GO has a lower Young's modulus (for example, Suk et al. reported a value of 207.6 ± 23.4 GPa [55]). The attached oxygen groups inhibit electrical conductivity, thus increasing its resistivity. [56] In contrast to graphene, GO has a low thermal conductivity $K = 0.5 - 1 \text{ W m}^{-1} \text{ K}^{-1}$. [57]

Similarly to the graphene preparation, starting material for a GO synthesis is graphite. Graphite oxidation has been examined since 1859 when British chemist Brodie performed a reaction of graphite with potassium chlorate (KClO_3) in fuming nitric acid. [58] The created material was dispersible in pure water or basic solution. A further improvement of the reaction was made by a chemist Staudenmaier 40 years later. He added KClO_3 in multiple aliquots during the reaction instead of one addition at the start. [59] Finally, Hummers and Offeman used potassium permanganate (KMnO_4) instead of chlorate as an oxidation agent, which they dissolved in sulfuric acid (H_2SO_4). [60] Both Hummers and Stauden-

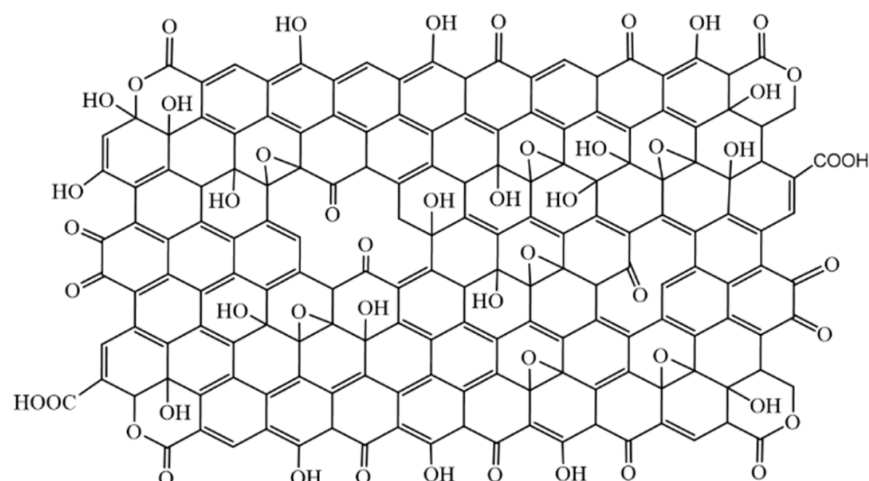


Figure 3: Graphene oxide structure with various oxygen containing groups. [67]

maier methods are the most common and currently used ways of graphite oxidation. Note that the final product and composition does not depend solely on the chosen method but also on the graphite quality and reaction conditions. [53] Finally, the last widely used method is the exfoliation of graphite oxides. Exfoliated GO can be dispersed by sonication in pure water thanks to its hydrophilic character. The final product is a yellow GO suspension. [61] GO-based materials can be used in a water treatment, thanks to the high water permeance of GO. [62] A sponge material made by a hydrothermal treatment of GO dispersion has high adsorption ability for various dyes, oils, and organic solvents. [63] GO-based electrodes were reported with a high specific capacitance 401 F g^{-1} in aqueous electrolytes. [64] Thanks to the preparation by using wet chemistry, it is easy to deposit graphene oxide on the substrates, which creates an interesting electrode material. [65] Finally, GO can be used for a gas separation. [66]

2.2.3 Fluorographene

A stoichiometric derivative of graphene with attached fluorine atoms is called fluorographene (FG). The attachment of the fluorine to carbon atoms prolongs the C—C bond to the length of 0.156 nm. [68] Young's modulus is $E = 0.3 \text{ TPa}$. [69] FG is a hydrophobic material, similarly to its 1D counterpart Teflon. The thermal decomposition starts at a temperature range of $400\text{--}600 \text{ }^\circ\text{C}$. All carbons are sp^3 hybridized, and therefore FG loses the delocalized electron clouds. Whereas graphene is known as the thinnest conductor, fluorographene is the

thinnest insulator with the band gap up to 8.3 eV. [68, 70]

Fluorographene can be prepared by an exfoliation of graphite fluoride, which is an industrial lubricant, and therefore it is available in large quantities. The mechanical exfoliation is not suitable for a large-scale production because of the time consumption. [69] A more appropriate approach appears to be a liquid-phase exfoliation. Graphite fluoride dissolves in the solvents as sulfolane [71], N,N-dimethylformamide [72], and various ionic liquids (as 1-butyl-3-methylimidazolium bromide) [73] followed by ultrasonication.

However, it is possible to fluorinate graphene directly by fluorination agents. The most used agent is XeF₂. [74] In addition, elementary fluorine gas F₂ can be also used to create FG from pristine graphene or rGO. [75, 76]

Fluorographene has a potential for an application in areas such as batteries and supercapacitors, a carbon-based magnetic resonance imaging contrast agent, (bio)sensors for biochemically relevant molecules, and dye-sensitized solar cells. [44, 77, 78] However, the most interesting is the reactivity of the material that will be discussed in more detail in the next chapter.

2.2.4 Cyanographene

Graphene covalently modified by nitrile groups is known as cyanographene (GCN) or graphene nitrile. The only established method of its synthesis is through a nucleophilic substitution of FG by NaCN in DMF, which substitutes some fluorine atoms by CN groups, and eliminates others, which leads to the formation of C=C bonds. Therefore, the final product is non-stoichiometric with a degree of functionalization around 15 % and with re-established delocalized π -electron cloud, thus unlike fluorographene, GCN is a conductor. [79]

GCN is a promising material for the catalytic application, where an anchored platinum atom on the surface of GCN allows its usage in the single-atom catalysis. [80]

2.2.5 Graphene acid

So far, two preparation routes to graphene derivatives with attached carboxyl groups were reported. First, multiple oxidations of graphite by a permanganate led to formation of graphene oxide followed by further oxidation to graphene acid. This created a graphene lattice with multiple defects, where almost every carbon was bonded to a carboxyl group. Because of the harsh conditions of oxidation, final properties could not be precisely defined. For example, the value of pK_a was in the range 2 – 4.5, depending on the number of carboxylic groups. This graphene acid could be used as a filtration material for liquids with ions of heavy metals. [81]

A different approach towards the synthesis of graphene acid was discovered in 2017 through the hydrolysis of GCN. As it is known from organic synthesis, nitrile groups can be hydrolyzed by reaction with dilute acid, and therefore it is possible to create graphene acid by submerging GCN into 20% HNO_3 . Graphene acid from this reaction is covered only by carboxyl groups and without defects in the graphene lattice. Because hydrolysis is not as harsh as oxidation with permanganate, the final properties are better determined. For example, the acid formed by hydrolysis has $pK_a = 5.2$, and therefore the chemistry of this acid is well-defined in contrast to several times oxidized graphene. It was shown that graphene acid is in suspension exfoliated only when $pH > pK_a$ and carboxylate groups are dissociated. On the contrary, with pH lower than pK_a , carboxylates can create interlayer hydrogen bonds. Hence, changes in pH can be used for reversible agglomeration or exfoliation of graphene acid (Figure 4). The derivative has a low toxicity and high biocompatibility [79], and can be used for a selective base to sensors, e.g., for the detection of H_2O_2 [82], or electrochemical sensing of biomarkers [83].

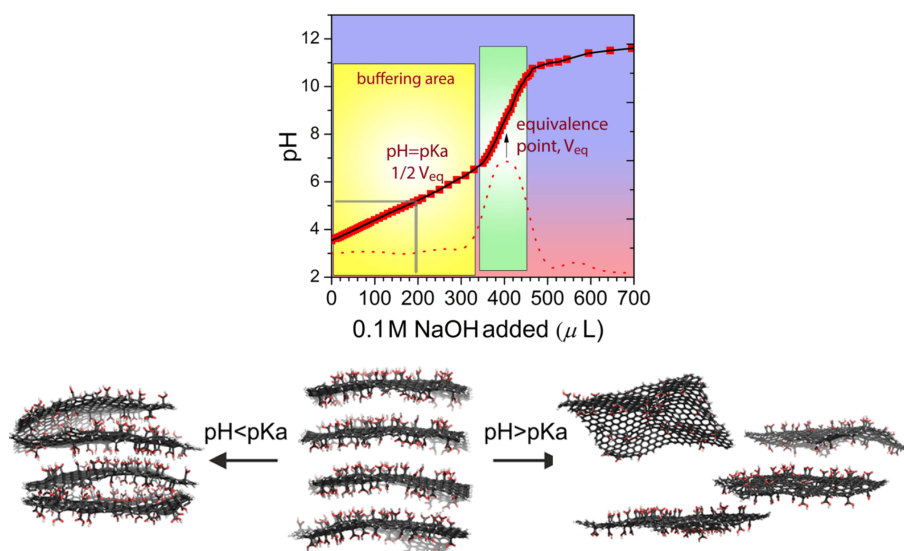


Figure 4: Titration curve of graphene acid, and stacking of graphene sheets with a change of pH . [79]

2.3 Reactivity of graphene derivatives

As discussed above, graphene is exceptionally chemically inert material and it is usually considered as nonreactive. However, as was described, methods of its derivatization were developed. In the next chapter, the chemistry of graphene oxide, fluorographene, graphene acid, and cyanographene will be described in more detail.

2.3.1 Graphene oxide

As it was shown, graphene oxide contains various types of oxygen groups. Its carboxyl groups can undergo esterification or create amid bonds [84, 85]. Additionally, epoxy groups on the surface of GO can be opened by a nucleophilic attack. The reaction of octaldecylamine with GO dispersion opens the epoxy rings and forms a product of amine with neighboring hydroxyl groups. [86]

Further, GO can be reduce; the topology of the final product depends the method of the reduction. Pumera et al. studied graphene oxide produced by Staudenmaier's method, which was reduced by lithium aluminum hydride ($LiAlH_4$), hydrazine (N_2H_4), and sodium borohydride ($NaBH_4$). Oxygen content in rGO decreased after the reaction in all cases. It should be noted that the reaction with hydrazine led to the incorporation of nitrogen impurities into

rGO. The main difference between the reducing agents was the number of carboxyl groups left after the reduction. LiAlH_4 was able to reduce more carboxyl groups than N_2H_4 and NaBH_4 . Table 1 summarizes results of the reduction. [87]

Table 1: Results of three reduction procedures. Each reduction was performed with a different reducing agent. The material 28.2 % oxygen mass content was reduced to 12.3, 10.4 or 10 % respectively. A small portion of the original amount of carboxyl groups remains even after the reduction. [87]

| | Red. agent | w/w of O | Left -COOH |
|--------------|------------------------|-----------------|-------------------|
| rGO 1 | NaBH_4 | 12.3 | 6 % |
| rGO 2 | N_2H_4 | 10.4 | 7 % |
| rGO 3 | LiAlH_4 | 10.0 | 2 % |

Note that the reduction by LiAlH_4 is performed in the THF. However, GO from its nature contains some moisture, hence LiAlH_4 molecules can potentially react with the residual water and create a locally strong basic environment that results in the evolution of a H_2 gas. In any case, reduction properties of the LiAlH_4 on GO was observed. [87]

Reduction by LiAlH_4 was reported even for functionalized GO. GO can react with sodium azide (NaN_3), which leads to azide-functionalized GO, which can be also reduced by LiAlH_4 to amino-functionalized graphene oxide. [88, 89]

2.3.2 Fluorographene

Surprisingly, fluorographene is nowadays the most used precursor for following graphene functionalization. From an organic chemistry point of view, fluorographene is a perfluorocarbon. Organic molecules containing only carbon and fluorine are considered as nonreactive and chemically inert entities. However, it was shown that fluorographene can undergo a reaction with KI, which leads to metastable graphene iodide, followed by an immediate decomposition to pristine graphene and I_2 . [71] In the following years, the reductive defluorination of FG was discovered by the reaction with triethylsilane or zinc nanopowder. [72] The reason for this originally unexpected reactivity was found in the semi-ionic character of the C—F bond. [70] Furthermore, DFT calculations together with EPR and NMR experiments discovered a radical reaction mechanism triggered by point defects in the FG

structure. [90] The absence of these defects in the Teflon structure is probably a reason for a different reactivity between 1D and 2D counterparts.

A whole range of nucleophilic substitution reactions was performed since the discovery of fluorographene. These reactions led to a new class of graphene derivatives (some of them were already introduced). One of the first nucleophilic substitutions was the FG reaction with ethylenediamine, which attached amine to the graphene surface. This allowed further functionalization through the second terminal amine group. [91] Besides N-nucleophiles, S- and O-nucleophiles have been applied for a FG functionalization. The reaction with alcohol ($R-OH$) led to the creation of an etheric bond between oxygen and graphene. In contrast, organic S-nucleophiles act as a reducing agent removing fluorine atoms from FG without bonding themselves to graphene. [92] On the contrary, the reaction with inorganic NaSH in DMF creates thiofluorographene. [93] Attachment of alkynes or aryls is possible through a reaction of FG with Grignard reagents [94, 95] or via a recently reported Suzuki-Miyaura coupling reaction. [96] Hydroxylated graphene can be prepared by a reaction of FG with alkali. [97] All reactions are accompanied by the reduction of some FG carbons by a spontaneous defluorination and a creation of new double bonds; all the new derivatives are non-stoichiometric hence. FG subjected to NaCN in DMF solution creates graphene derivative covered with nitrile groups. [79] An overview of the individual reactions is graphically illustrated in Figure 5.

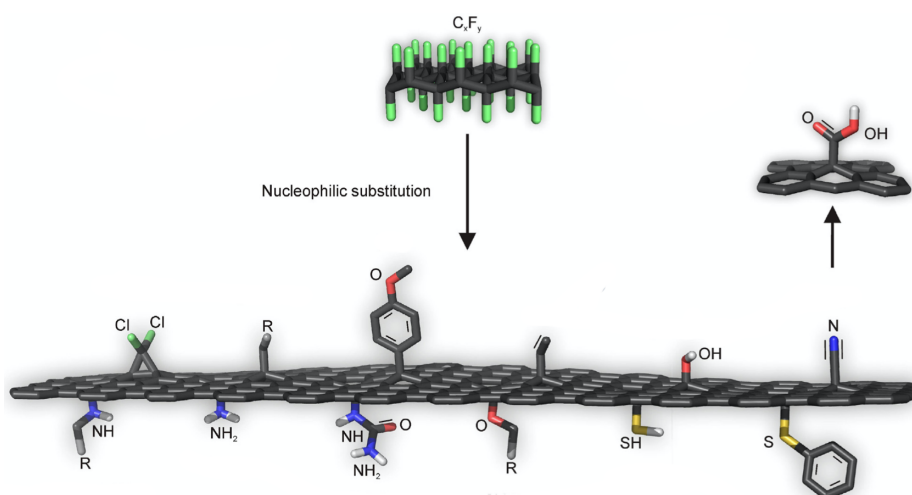


Figure 5: Reactions of fluorographene, which lead to a wide portfolio of graphene derivatives. [68]

Cyanographene and graphene acid

Despite the fact, that few reductions of the other functional groups (as a carboxyl group in graphene oxide or azide groups of azide functionalized graphene oxide) have been reported, the reduction of nitrile groups on the surface of GCN was reported only marginally. Despite the extensive addition of an acid solution into the reaction mixture, the hydrolysis step did not proceed completely, indicating a complicated behaviour in reacting with GCN. [98] The only other known reaction of GCN is its hydrolysis by 20% HNO_3 , which leads to graphene acid. [79]

Graphene acid prepared by hydrolysis of GCN can be used for a further functionalization of the graphene material. A carboxyl group can be modified through carbodiimide chemistry, as it is shown in Figure 6. [79]

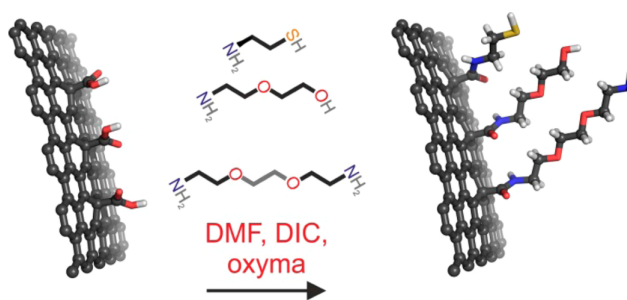


Figure 6: Functionalization of graphene acid with N-nucleophiles with terminal function groups on the other side. [79]

3. Methods

3.1 Computational chemistry

Computational chemistry has become an inseparable part of modern chemistry. Even with never-stopping improvements in experimental methods, it is still impossible to obtain all relevant information about the molecular system. This gap is bridged with the help of computational chemistry, which uses mathematical methods combined with laws of physics to study chemical systems. Furthermore, computational chemistry can be separated into two main approaches, *ab initio* quantum chemistry (QM) methods and empiric molecular mechanics (MM).

QM methods can be generally separated into two main areas, based on the type of approximation: *wave function theory* (WFT) and *density functional theory* (DFT).

The core of WFT is a wave function that fully describes the examined system. WFT can be applied to obtain information about the system by solving the Schrödinger equation. However, analytically solvable systems have to contain only two interacting particles (for example, a hydrogen atom), due to the correlated motion of the particles. Generally, this problem is simplified by Born-Oppenheimer approximation, which decouples the motion of electrons and nuclei and computes electronic energies for fixed nuclear positions. Further, *Hartree-Fock* (HF) method approximates the molecular wave function as a product of one-electron functions. HF is then the starting point for more complex methods, so-called post-HF methods.

On the other hand, DFT uses Hohenberg–Kohn theorems, which say that the properties of multielectron systems are fully-described by the electron density in the molecules. Nowadays, DFT is used more frequently than WFT methods because its computational demands are similar to the basic HF methods, but the accuracy of the results is on the level of more complex post-HF methods. [99, 100]

Nevertheless, only systems with tens or hundreds of atoms can be computed by using QM methods. A completely different approach needs to be used in order to compute chemical systems containing thousands of atoms. One of them is called *molecular mechanics*, which will be discussed in the following text. [101]

3.2 Molecular mechanics

Molecular mechanics or *force field method* allows performing simulations with large and complex structures, such as proteins, nucleic acids, or nanomaterials. However, the growing size of the system is compensated by the order of the approximations. The most important simplification is the neglect of an electron structure of molecule. Furthermore, following Born-Oppenheimer approximation, the quantum character of the nuclear motion is also not considered.

This level of approximation allows to model systems with laws of classical mechanics. MM is an empiric method and therefore uses parameters obtained from high accurate QM calculations or from the experimental data. These sets of parameters with equations describing the system are called *force field* (FF), hence the name of the method. Different molecules can be built from similar "building blocks" (for example, a methyl group is similar in two different molecules). Therefore it is possible to utilize one FF to model a series of related systems rather than define a set of new parameters. This feature of FF is called *transferability*. [101, 102]

Generally, classical systems are represented by spheres connected with a harmonic oscillator, and the total potential energy of the system is a function of atomic coordinates. Each atom is classified by *atom types*, which describe its hybridization and chemical surroundings. For example, a different atom type can be used for carbon in an aliphatic chain and another type for carbon in a carboxyl group. [102]

Equation 1 shows five basic terms (divided into covalent and non-covalent terms) of the potential energy, although, additional terms can be included in a more complex force field (e.g., terms for polarization, three-body interactions,...).

$$E_{\text{total}} = E_{\text{covalent}} + E_{\text{noncovalent}} = E_{\text{bonds}} + E_{\text{angles}} + E_{\text{torsions}} + E_{\text{vdW}} + E_{\text{els}}. \quad (1)$$

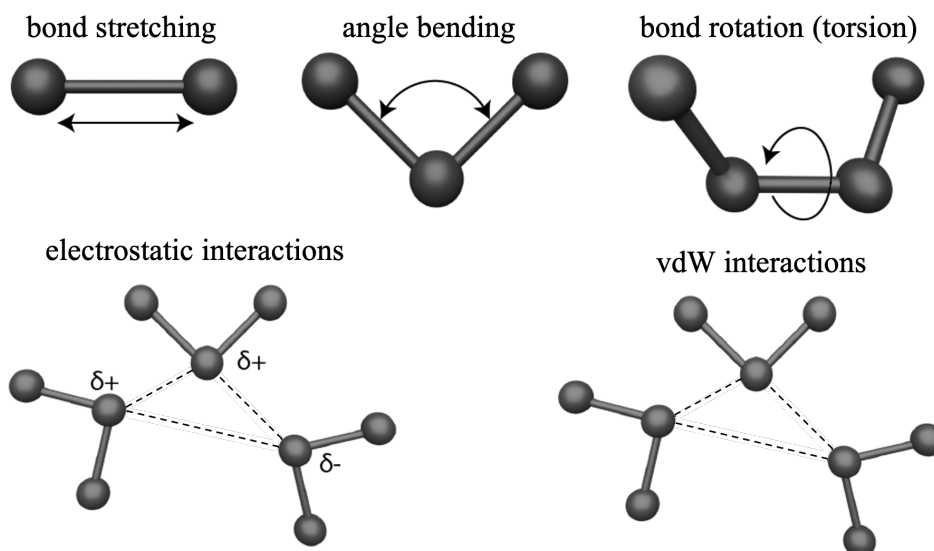


Figure 7: Schematic illustration of the fundamental force field energy terms.

3.2.1 Covalent terms

Generally, covalent terms can be divided into 3 types: bond stretching, bending of angles between atoms, and a torsional energy for rotation around a bond.

Bonds in the most simplest cases can be described by Hooke's law (equation 2)

$$E_{\text{bonds}} = \sum_{\text{bonds}} \frac{k_b}{2} (b - b_0)^2. \quad (2)$$

b_0 is the reference length, where the energy of the bond is minimal, b is the length of the bond, and k_b is the force constant of the bond, describing its "stiffness".

Equation 2 is describing harmonic oscillator (i.e., the energy goes to infinity when the bond is extremely stretched), and thus one cannot expect an accurate description of processes where the bonds are near the bond breaking separation (i.e., the bond is distant from the reference length). A better description of an anharmonic bond character can be in more advanced force fields obtained by *Morse potential* (the difference between the harmonic and anharmonic potential is pictured in Figure 8). The potential converges to dissociation energy D_e with stretching of the bond.

$$E_{\text{bond}} = D_e (1 - e^{-a(l-l_0)})^2, \quad (3)$$

where a is based on the force constant of the bond:

$$a = \sqrt{\frac{k}{2D_e}}, \quad (4)$$

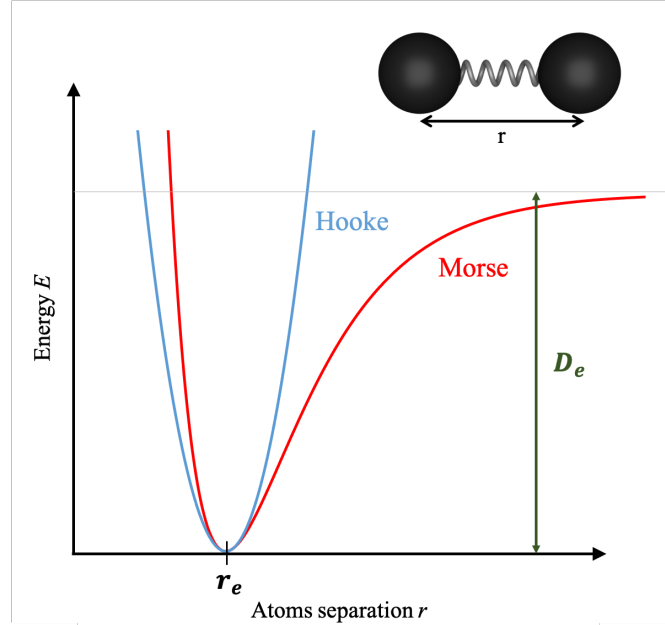


Figure 8: Comparison of the anharmonic Morse potential (red) a harmonic oscillator described by Hooke's law (blue).

The next term describes the energy required for bending an angle between three atoms. Similarly to E_{bonds} , the deviation of angles from reference value θ_0 is described by a harmonic potential:

$$E_{\text{angles}} = \sum_{\text{angles}} \frac{k_{\theta}}{2} (\theta - \theta_0)^2, \quad (5)$$

where k_{θ} (correspondingly to bond stretching) is the force constant, describing how hard it is to deviate the angle from its reference.

Last covalent term is connected with the change of torsion angle ω between four atoms

$$E_{\text{torsion}} = \sum_{\text{torsions}} \frac{V_n}{2} [1 + \cos(n\omega - \gamma)], \quad (6)$$

V_n describes the size of the energy barrier, n is multiplicity that is related to a number of minimum points in the function, and the position of minimum points is determined by the phase factor γ . [101, 102]

3.2.2 Non-covalent terms

Basic non-covalent terms are of two types. First term describes electrostatic interaction. Electrostatic potential is calculated by Coulomb law based on atomic charges q_i :

$$E_{\text{els}} = \sum_{i < j} \frac{1}{4\pi\epsilon_0\epsilon_r} \frac{q_i q_j}{r_{ij}}, \quad (7)$$

where ϵ_0 is the vacuum permittivity, ϵ_r is a relative permittivity and r_{ij} is a distance between atoms.

Second non-covalent term describes van der Waals (vdW) interactions. These interactions can be both repulsive and attractive. vdW interactions converge to zero at large interatomic distances. On the other hand, if atoms get too close to each other, vdW interactions become strongly repulsive. However, at intermediate distances, atoms can slightly attract each other. The most used function for vdW interaction description for the MM purpose is the *Lennard-Jones 12-6 potential* (LJ):

$$E_{\text{vdW}} = \sum_{i < j} 4\epsilon_{ij} \left[\left(\frac{\sigma_{ij}}{r_{ij}} \right)^{12} - \left(\frac{\sigma_{ij}}{r_{ij}} \right)^6 \right]. \quad (8)$$

The LJ function has only two parameters. The depth of the minimum ϵ_{ij} and the distance, where the energy of the interaction is zero (so-called collision diameter) σ_{ij} . A graphical illustration of LJ potential is shown in Figure 9.

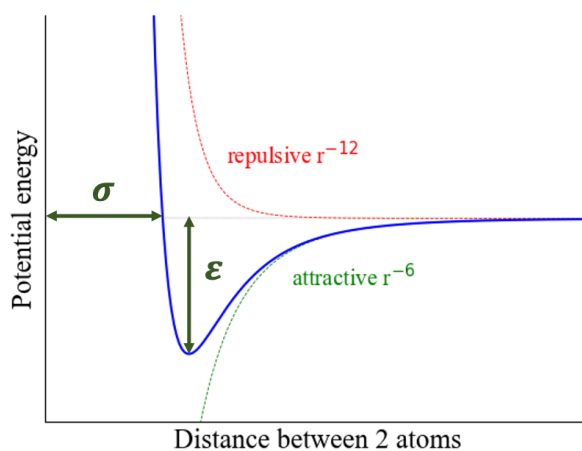


Figure 9: The Lennard-Jones potential.

LJ parameters σ_{ij} and ϵ_{ij} depend on both atoms. Although these parameters in FF are written in terms of individual atom types σ_{ii} and ϵ_{ii} , di-atomic parameters can be combined from them by *mixing rules*. *Lorentz-Berthelot combining rules* that are used by the most common FF for biomolecules, calculate the collision diameter σ_{ij} as the arithmetic mean of the values for two pure species [102]:

$$\sigma_{ij} = \frac{\sigma_{ii} + \sigma_{jj}}{2}, \quad (9)$$

and depth ϵ_{ij} is given as the geometric mean:

$$\epsilon_{ij} = \sqrt{\epsilon_{ii}\epsilon_{jj}}. \quad (10)$$

Effective potential

An interaction between two atoms can be affected by the presence of other particles, so final potential energy between three molecules **A**, **B** and **C** is not often given by a simple summation of pairwise interactions:

$$E(\mathbf{A}, \mathbf{B}, \mathbf{C}) \neq E(\mathbf{A}, \mathbf{B}) + E(\mathbf{A}, \mathbf{C}) + E(\mathbf{B}, \mathbf{C}) \quad (11)$$

This is known as the *three-body effect* (*many-body effect* in the case of more particles). The three-body dispersion formulas are known, and the three-body Axilrod-Teller contribution is presented as an example.

$$E^{(3)}(\mathbf{r}_{AB}, \mathbf{r}_{AC}, \mathbf{r}_{BC}) = E_{A,B,C} \frac{3 \cos(\theta_A) \cos(\theta_B) \cos(\theta_C)}{(\mathbf{r}_{AB}\mathbf{r}_{AC}\mathbf{r}_{BC})^3}. \quad (12)$$

Despite the known formula for three-body interactions, its usage would mean a dramatic increase in time needed to complete the simulation because a system with N particles has approximately $N/3$ times more three-body terms than two-body ones. [102] One way, how to overcome this problem is by incorporating many-body effects into parameters of the force field themselves. Thus the pair potentials in the common force field are *effective potential*. For example, the polarization of molecules can be implicitly included in FF by overestimation of the electrostatic interactions.

However, the polarization can be also introduced into the system explicitly by *Drude oscillator model*. This represents the polarization in the molecules by adding a massless charged particle attached to the considered atom by a harmonic spring. The distance between the

atom and Drude particles self-consistently adjusts itself to energy minima based on the configuration of surrounding atoms and gives molecules their dipole moment. [103]

Partial charges

A large contribution to atomistic forces is based on the interaction between charges, thus they need to be correctly assigned to molecules. However, partial charges are not experimentally observable quantities, and furthermore, they even cannot be determined by using the Schrödinger equation. However, various methods can be employed for their assignment. The partial charges can be obtained from fitting to known molecular dipole moments, from the Mulliken population analysis of atomic orbitals, or by assigning atom charges by reproducing experimental results. [100]

Another way how to assign charges is the reproduction of an electrostatic potential (ESP) around the molecule. Since the electrostatic potential is an observable quantity and can be calculated from the wave function, a large number of points with a known electrostatic potential around the molecular surface can be created. After obtaining of a grid of points with known a electrostatic potential, a least-square fitting procedure assigns partial charges to atoms, which best reproduces electrostatic potential at the points. In the end, the sum of all partial charges has to be equal to the charge of the whole molecule.

A modified version of ESP is used for the simulation with an AMBER force field. *Restrained electrostatic potential* (RESP) applies hyperbolic restraints on non-hydrogen atoms. Calculations with QM are commonly proceeding with the HF level 6-31G* basis set. This method is less dependent on the conformation of a molecule and creates smaller charges on the buried atoms. [100, 102, 104]

3.3 Molecular dynamics

Because of the neglect of the electronic structure, the time evolution of MM systems can be studied by classical Newton's physics. This process is called *molecular dynamics* (MD). The acceleration is the second derivation of the coordinates with respect to time, so the Newton's second law ($F = ma$) can be written as the differential equation:

$$F_i = m_i \frac{d^2 x_i}{dt^2} \quad (13)$$

Moreover, the force is enumerated as the negative gradient of the potential energy:

$$F_i = -\nabla_i E(\mathbf{r}_1, \mathbf{r}_2, \dots, \mathbf{r}_n). \quad (14)$$

By solving equation 13, we can generate a set of time-correlated points in the phase space, called *trajectory*. [102, 105]

The force acting on each particle varies with every change in the system. Hence, the motion of all atoms is coupled together. As a result, it is impossible to solve motion equations analytically, and therefore numerical methods have to be applied. In that case, equations of motion are integrated by using *finite difference method*.

The integration is divided into small steps, each separated by a fixed time Δt (called *time step*). A force applied on a particle at time t is obtained as the vector summation of all interactions acting on it. If forces acting on the particle are known, the acceleration of the particles can be calculated. From the above, it is possible to find new positions and velocities of particles at the new time $t + \Delta t$. The applied force is constant during this time step, and therefore, the Δt has to be chosen with care, e.g., a large time-step would make the system unstable. On the other hand, a disproportionately small time step means that more (unnecessary) steps are needed to propagate the system into the final stage. [105]

One of the most used algorithms is *The Verlet algorithm*. This algorithm uses the positions and accelerations at time t , and the positions from the previous step $\mathbf{r}(t - \Delta t)$ to propagate particle into the new position at $t + \Delta t$. It is assumed that the positions and dynamic properties can be approximated as Taylor series expansions:

$$\mathbf{r}(t + \Delta t) = \mathbf{r}(t) + \Delta t \mathbf{v}(t) + \frac{1}{2} \Delta t^2 \mathbf{a}(t) + \dots \quad (15)$$

$$\mathbf{r}(t - \Delta t) = \mathbf{r}(t) - \Delta t \mathbf{v}(t) + \frac{1}{2} \Delta t^2 \mathbf{a}(t) - \dots \quad (16)$$

These two equations can be summed together to get the final one:

$$\mathbf{r}(t + \Delta t) = 2\mathbf{r}(t) - \mathbf{r}(t - \Delta t) + \Delta t^2 \mathbf{a}(t) \quad (17)$$

The drawback of the equation 17 is the fact, that the final position $\mathbf{r}(t + \Delta t)$ is obtained by adding a small term $\Delta t^2 \mathbf{a}(t)$ to the difference of two larger numbers. Furthermore, since the Verlet algorithm propagates the system with no reference to the velocity, this integration method can be used only when the velocity-independent properties are studied. [102]

Additionally, the default option for the integrator in Gromacs software is the modification of the Verlet algorithm called *leap-frog*. This algorithm uses positions $\mathbf{r}(t)$ and velocities $\mathbf{v}(t - \frac{1}{2}\Delta t)$, which is a one-half time step out of phase. Following equations show the leap-frog relation for the velocity

$$\mathbf{v}\left(t + \frac{1}{2}\Delta t\right) = \mathbf{v}\left(t - \frac{1}{2}\Delta t\right) + \frac{\Delta t}{m}\mathbf{F}(t), \quad (18)$$

and for the position

$$\mathbf{r}(t + \Delta t) = \mathbf{r}(t) + \Delta t \mathbf{v}\left(t + \frac{1}{2}\Delta t\right) \quad (19)$$

The leap-frog name of the algorithm comes from velocities "jumping" over positions to give their value at $t + \frac{1}{2}\Delta t$ (Figure 10). [106, 107]

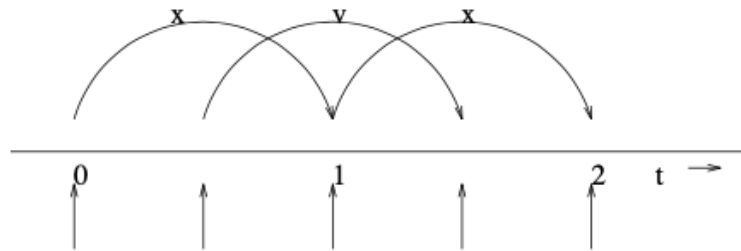


Figure 10: Schematics of the leap-frog algorithm, commonly used by the Gromacs software. [107]

Radial distribution function

Generally, distribution functions describe the value of the observable property as a function of an independent variable. One example is a *radial distribution function* (RDF), which describes the probability of finding the particle as a function of distance from another atom (or molecule) compared to the expected occurrence from a completely uniform distribution (ideal gas with density N/V):

$$g(r, \Delta r) = \frac{V}{N^2} \frac{\langle N(r, \Delta r) \rangle_M}{4\pi r^2 \Delta r} \quad (20)$$

$N(r, \Delta r)$ is the number of particles in between r and $r + \Delta r$ from another particle, and a spherical shell volume with the thickness Δr is expressed as $4\pi r^2 \Delta r$. [101, 102]

Periodic boundary condition

The *periodic boundary condition* (PBC) can be employed in order to overcome problems with solvent surface effects. The simulation box is surrounded by copies of itself, which are duplicated in all direction. This cause that the number of solvent molecules is preserved through the whole simulation, because if molecule leaves the box, its copy comes from the replica (as shown in Figure 11). Furthermore, 2D materials can be simulated as an infinite crystal, and the effect of its edges can be neglected. [102]

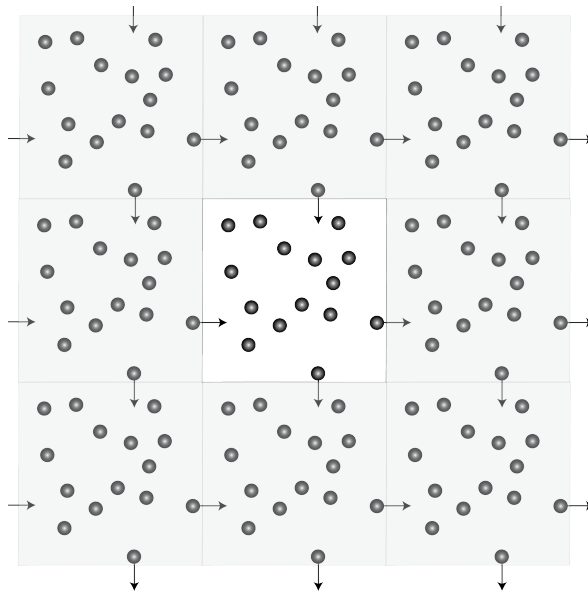


Figure 11: Graphical representation of periodic boundary condition.

4. Reduction of cyanographene

One of the newest and the most promising graphene derivatives is cyanographene, which can be prepared by reaction of fluorographene with NaCN in DMF. A nitrile group is a well-known group in organic chemistry, with the established reducing procedure by lithium aluminum hydride (LiAlH_4). However, as was mentioned above, the amine conversion on GCN was reported marginally with only partial conversion. [98]

In the present thesis, I used classical molecular dynamics simulations to examine the mechanistic part of the reduction reaction of GCN and aliphatic nitriles in THF by LiAlH_4 . I focused purely on the mechanical and steric contributions of the reduction reaction. Undoubtedly, chemistry behind the reaction mechanism is the decisive factor of the reduction process. However, pure steric effects may be significant, at least in the systems containing 2D materials; the accessible space of reactive species may be considerably restricted in the case of graphene and graphene-like 2D materials. To gain deeper insight into the problematic of cyanographene reduction, the simulation with a 2D surface was compared with aliphatic molecules.

First, starting reaction state of the reduction reaction of the nitrile group will be discussed. The proper alignment of the reduction was prior described in the literature by DFT calculations. The role of the solvent will be discussed afterward, followed by the analysis of THF arrangement on the graphene surface. Last, the access of the LiAlH_4 to the nitrile group grafted on different aliphatic molecules will be described.

4.1 Mechanism of the reduction

In the generally accepted mechanism of the reduction of nitrile group by LiAlH_4 (Figure 12) the hydride anion $[\text{AlH}_4]^-$ attacks the electron-poor carbon followed by the electron transport to nitrogen.

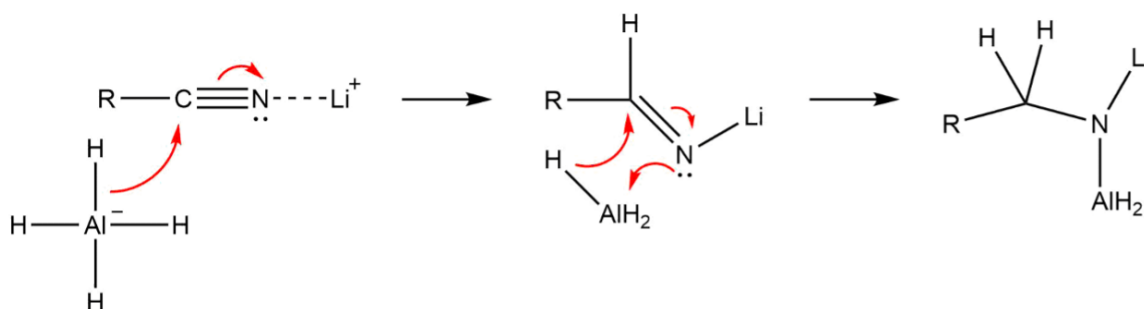


Figure 12: Reduction mechanism of nitrile by LiAlH_4 . [108]

A similar mechanism was also considered in the case of carbonyl functional group. Previous DFT calculations suggested the general configuration of the reaction state of the reduction of the carbonyl group in tetrahydrofuran. [109] It was shown that in order to initiate the reduction, LiAlH_4 has to be strictly aligned with the carbonyl group in one plane (see Figure 13) – with the torsional angle between C, O/N heteroatom, Li^+ and aluminum being close to zero. Moreover, in reactions involving carbonyl and nitrile, both groups are being attacked by a hydride atom, therefore similar spatial alignment can be assumed for the reduction reaction of the nitrile group by LiAlH_4 .

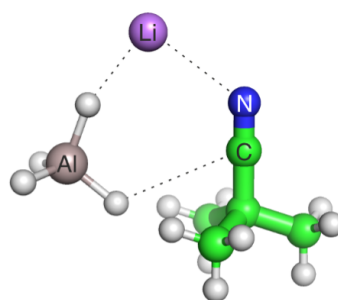


Figure 13: Reaction state of LiAlH_4 with nitrile group analogously to [109] with carbonyl group. Coloring scheme: green, carbon; purple, lithium; grey, aluminum; blue, nitrogen; white, hydrogen.

4.2 Simulations description

All simulations were carried out in Gromacs software package. [107] Gromacs 4.5.1 was used for simulations of aliphatic molecules whereas Gromacs 5.1.4 was used for GCN systems (flat bottom restrain had not been introduced until version 5). I used AMBER force field ff99 [110] for general description of the system. Graphene carbons were modelled as uncharged LJ spheres, with modified Cheng and Steele parameters for graphitic carbons. [111] Since only parameterized tetrahedral molecule of aluminum is $[\text{AlCl}_4]^-$, its parameters were taken from DREIDING force field. [112] Similar approach for other aluminum tetrahedral compounds was applied earlier in literature. [113] Smaller aliphatic nitriles were placed in box $3 \times 3 \times 3$ nm, and longer molecules in box $3.5 \times 3.5 \times 3.5$ nm. Graphene sheet was modeled as a periodic and was placed in the middle of $3 \times 3 \times 10$ nm box (Figure 14), with flat bottom restrain applied on aluminum 3.2 nm from the center of the simulation box in the z-direction to prevent collisions of LiAlH_4 molecules. In the starting geometry (all considered molecules are shown in Figure 15). One molecule of LiAlH_4 was added for each nitrile group, (thus one LiAlH_4 for aliphatic molecules and two molecules for graphene).

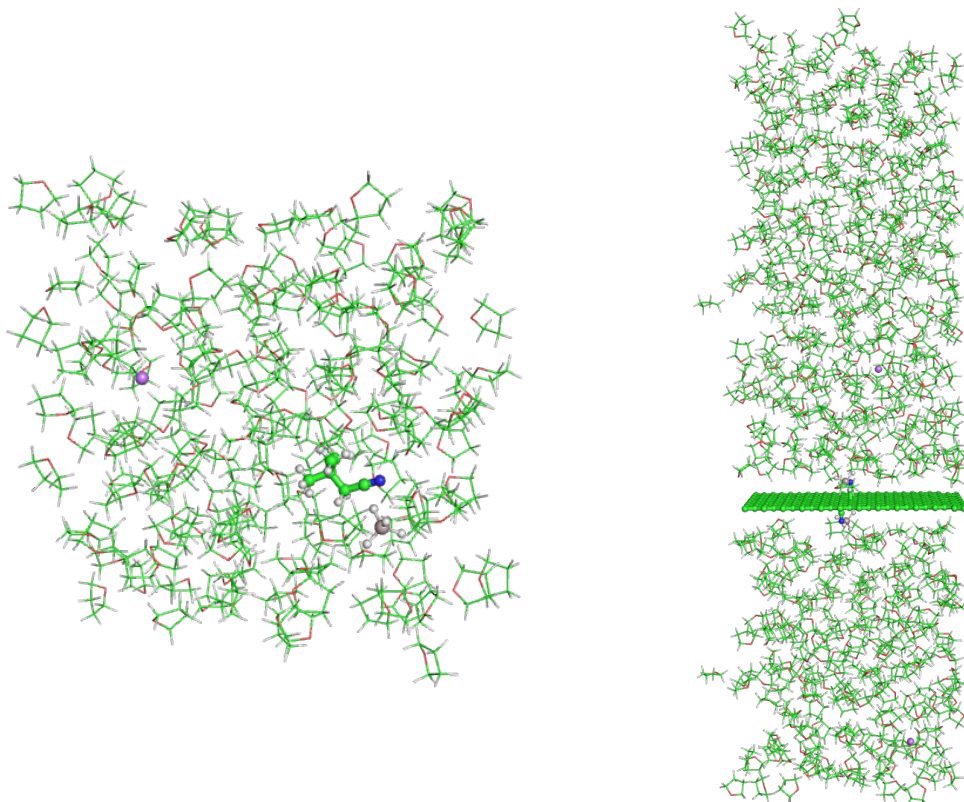


Figure 14: Simulation box with aliphatic molecule and graphene in THF.

All systems were minimized and thermalized to desired temperature of 300 K in the NpT ensemble prior to the production run under the NVT ensemble. Temperature and pressure were maintained using the Nose-Hoover thermostat and Parrinello-Rahman barostat (1 bar), respectively. LJ potential was used for calculation of pair interactions. Long-range electrostatic interactions were treated by using Particle-Mesh Ewald method (PME). Cut-off distances for nonbonded interaction and the real part of the PME were set to 1 nm. Newton's equations of motion were integrated by leap-frog algorithm with a time step of 1 fs. Bonds involving hydrogen were constrained by LINCS algorithm. Periodic boundary conditions were applied in all directions.

3 types of solvents were used - SPC water [114], dimethylformamide (DMF) [115, 116], and tetrahydrofuran (THF) [115, 116]. Free simulations with DMF and water were 100 ns long, and simulations with THF 300 ns. Detailed description of aliphatic nitriles will be discussed later. Additionally, for a better description of the graphene-induced arrangement of THF, a 100 ns simulation of pristine (unfunctionalized) graphene was used. First 50 ns of the simulations were treated as an equilibration stage and thus excluded from the final analysis.

4.3 Results and discussion

To investigate different reactivity of GCN with common organic nitriles, the accessibility of LiAlH_4 to nitrile groups grafted on graphene and on aliphatic chains with different length was compared. In total, 7 aliphatic structures and graphene with grafted nitrile groups (for more detail see Figure 15) were investigated using MD simulations THF. Additionally to solvent comparison, simulations with water and DMF with nitrile aliphatic molecules were performed.

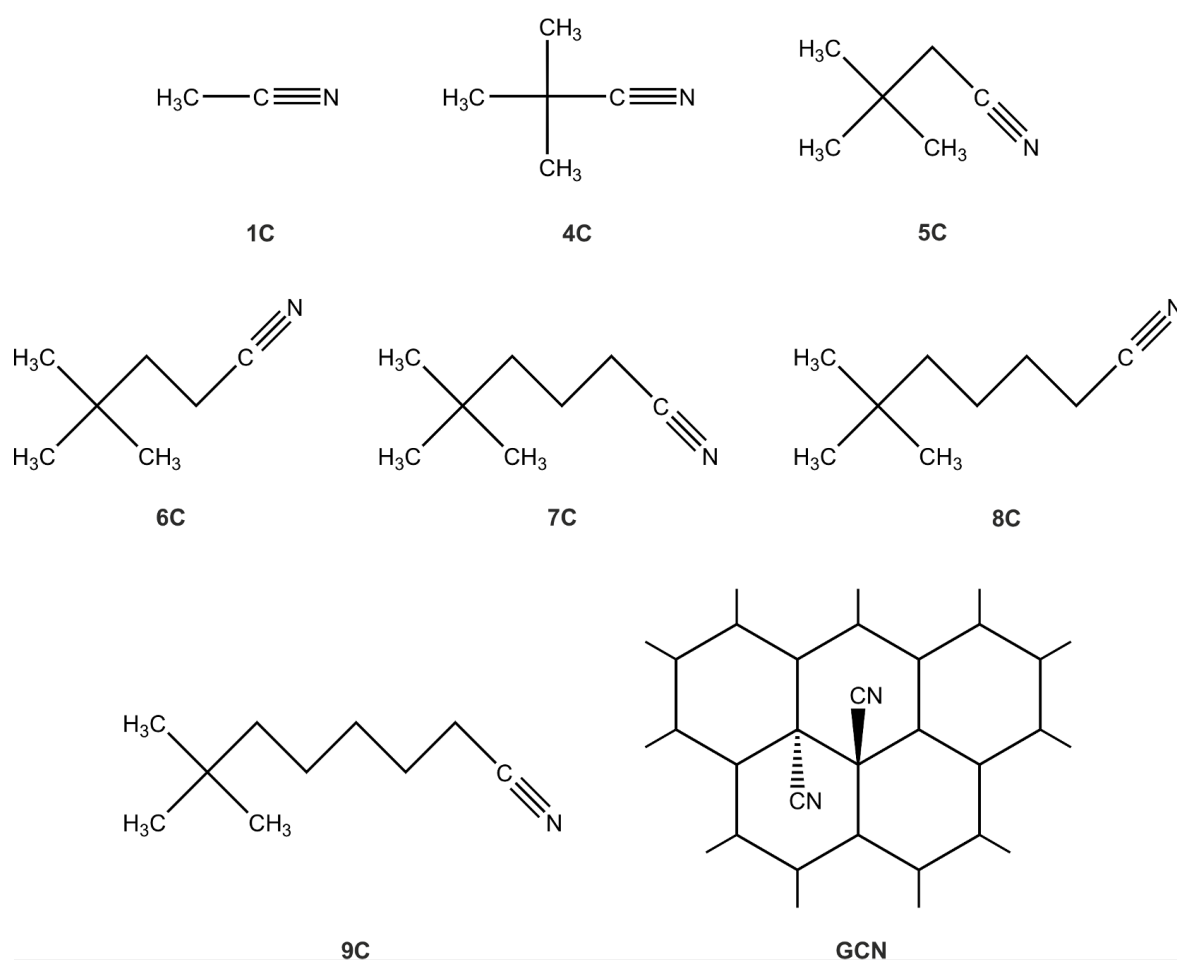


Figure 15: Considered structures of nitriles differing in aliphatic chain length. Numbering is derived from number of carbons in alkyl created by cleavage bond between carbon and nitrile group.

4.3.1 Differences in solvents

For a simple comparison, 100 ns simulations with all aliphatic structures in THF, DMF, and water were used. Neglecting the fact that LiAlH_4 can react with water and DMF, I focused solely on the different structures of the lithium aluminum hydride complex. The RDF between nitrogen from the 6C nitrile group and aluminum in all 3 solvents is shown in Figure 16. The occurrence of aluminum around nitrogen in 6C molecule in THF was larger than in bulk. On the other hand, both simulations, with water and DMF, did not show any increased occurrence around the nitrile group.

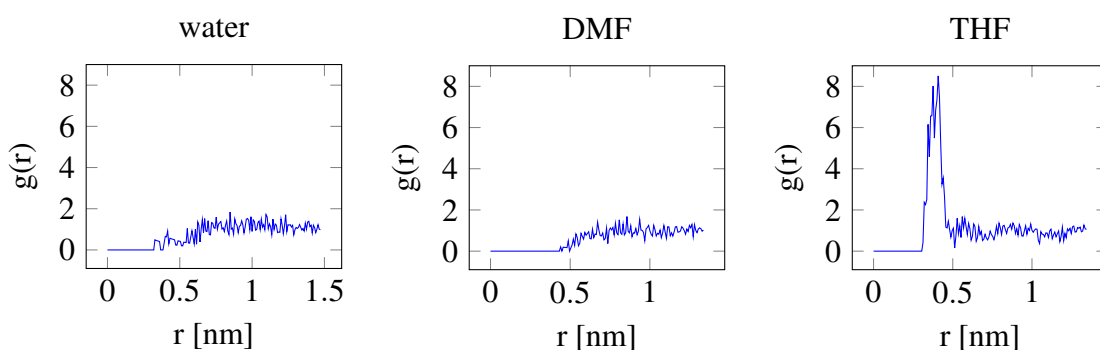


Figure 16: Radial distribution function $g(r)$ between nitrogen from nitrile group and aluminum in a) water, b) DMF and c) THF.

In all three simulations, LiAlH_4 had a different structure. In the water, the reducing agent was in the dissociated state. On the other hand, in both organic solvents, LiAlH_4 was in the associated state through the whole simulation. However, the less organized mutual organization was seen in DMF (Figure 17 for all three LiAlH_4 structures). Note, that arrangement of LiAlH_4 in THF, when lithium ion resides between two hydrides corresponds to the structure described by QM calculations in the literature. [109, 117] Nevertheless, in the following text, I will focus solely on simulation with THF, due to the inability of the reducing agent to access the functional group in more polar solvents.

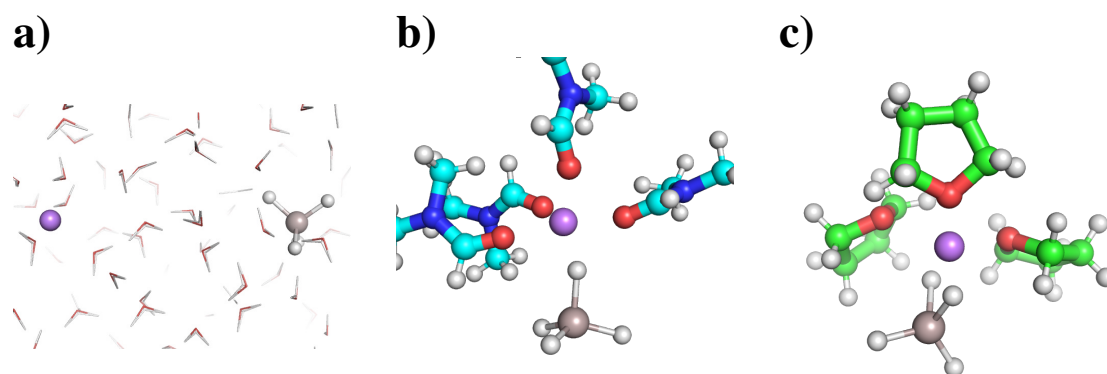


Figure 17: Structure of LiAlH_4 in a) water, b) DMF and c) THF.

4.3.2 Graphene-induced THF structuring

Since structuring of solvent is a largely discussed topic in the literature [118], I studied the arrangement of THF molecules induced by the graphene surface. From a 100 ns free simulation, I extracted the relative density of THF molecule around a graphene surface and their mutual orientation. Relative density of THF is shown in Figure 21 or in Figure S1. Similarly to other solvents, THF creates several distinct layers around graphene.

To determine the orientation of THF molecules in the first and second solvation layers, I assessed the angle defined by molecular plain vectors with respect to the surface (see Figure 18) (all molecules up to 0.7 nm from the surface were considered as the first layer; the second layer constituted from molecules between 0.7–1.4 nm from graphene). Molecules in the first layer showed parallel orientation to the graphene surface (because THF is not a planar molecule, the blue peak is slightly shifted from 90°). However, additionally, small peaks can be seen (at 160° , 50° and 130°). These peaks correspond to perpendicular T-shaped THF - graphene configuration.

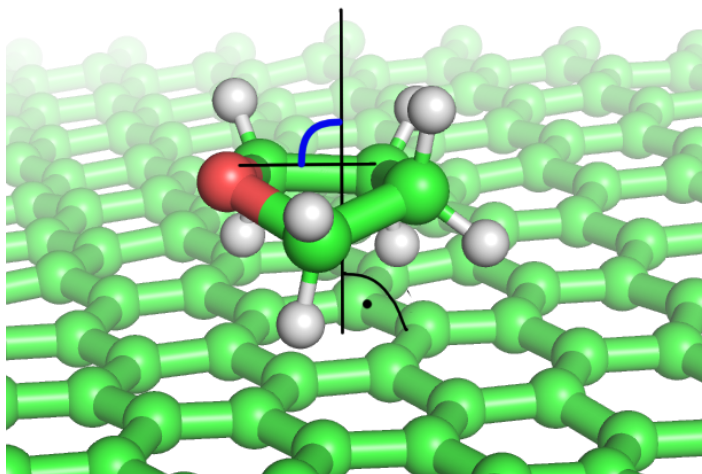


Figure 18: Measured angle between molecular plain vector and C - O vector in THF.

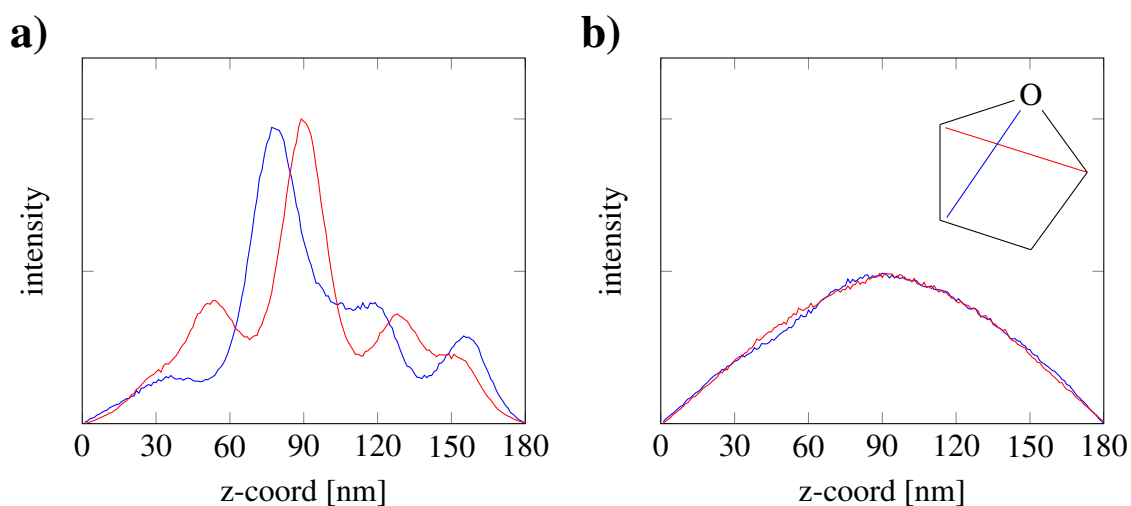
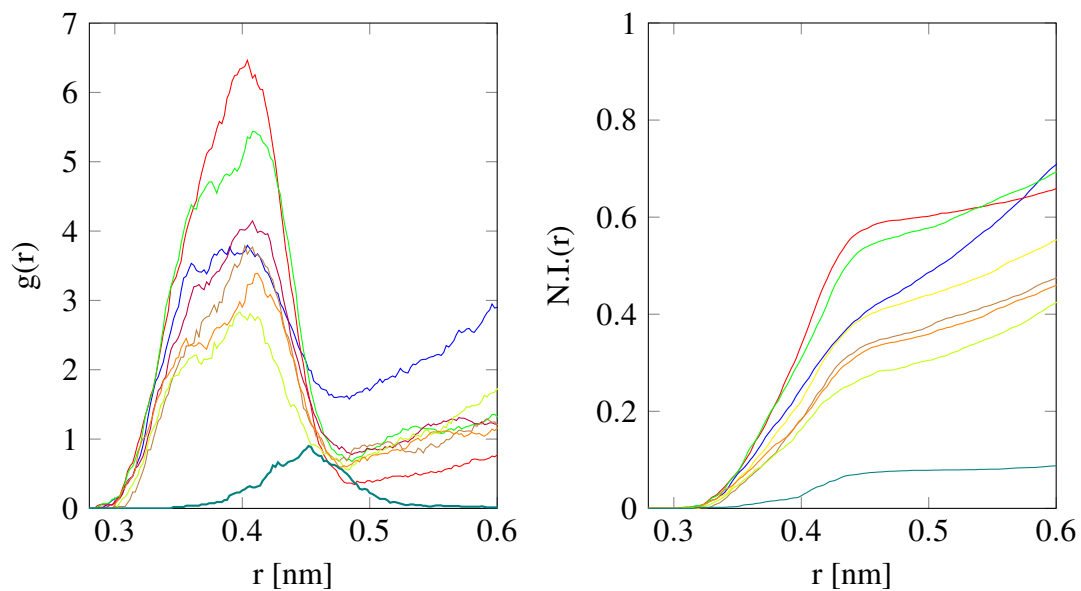


Figure 19: Orientation of the first a) and second b) layer of THF around graphene. In the insets both monitored vectors of the THF molecule are marked by a blue and red line.

4.4 Molecular accessibility of nitriles

The level of readiness of individual reactive components (LiAlH_4) to form the reaction state was inspected. RDF of aluminum with respect to the N or C atom of the nitrile group were calculated for seven aliphatic nitriles and GCN with the presence of LiAlH_4 in THF (Figure 20). They showed a general trend of decreasing accessibility of the nitrile group with the increasing alkyl chain in the aliphatic structure. Most likely, this trend originates from the free rotation of the carbon chain around single bonds resulting in the entropic repulsion of the hydride anion from the nitrile group. [119] Further, running integrals of RDF (Figure 20) started to grow at 0.3 nm. In almost all simulations integral radial distribution function of aluminum around nitrogen was larger than it was in the case of carbon. However, in the reduction of nitrile groups, the accessibility of the carbon is decisive as discussed previously. It is important to note that system with acetonitrile (1C molecule) has different characteristics, where carbon RDF was larger than nitrogen one. This was caused by the relatively unrestricted and easy approach of LiAlH_4 to the 1C molecule from the rear side (to the methyl group), where the distance between Al and C of the nitrile group can be smaller than 0.5 nm.

a)



b)

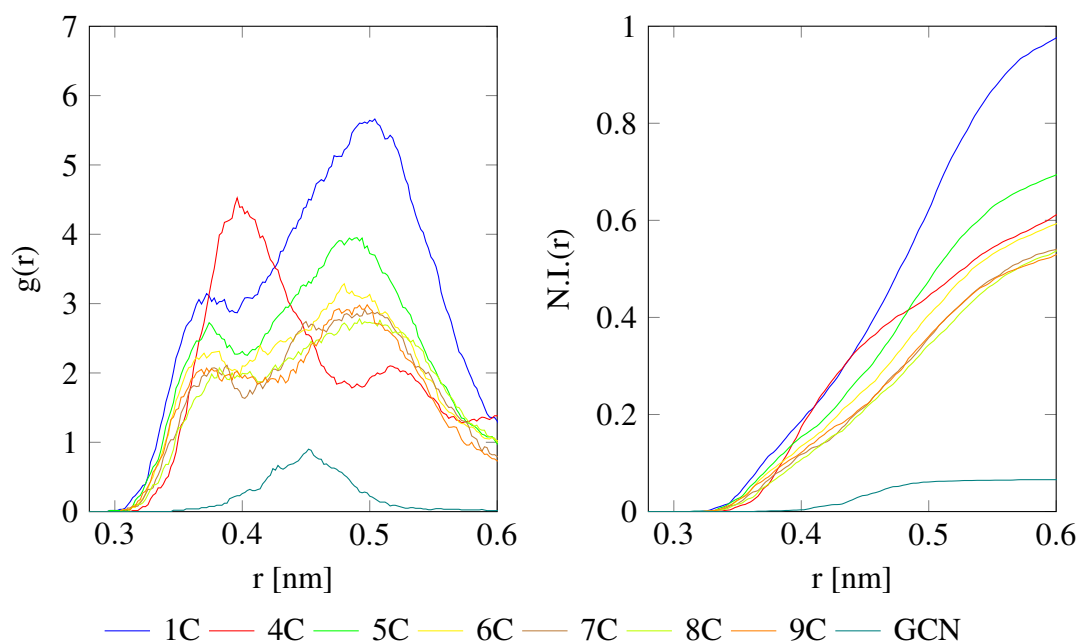


Figure 20: Radial distribution function $g(r)$ and its running integration numbers $N.I.(r)$ function between Al and a) N or b) C of the nitrile group. RDF were smoothed by moving average method.

On the contrary, the spacious tertial carbon in *tert*-butyl cyanide (4C) largely limited the final accessibility of $[\text{AlH}_4]^-$ in the immediate vicinity of the nitrile group. However, the terminal nitrogen in the 4C structure was not affected by the branched structure and reached a maximum in our ensemble. On the other hand, the biggest drop was observed in the case of GCN that could be attributed to the combination of several factors. Due to the strict solvent structuring around GCN the aluminum hydride was not able to enter the first solvent layer and mostly resided in the second THF layer (the mean distance of the aluminum atom from the graphene plane was 0.82 ± 0.1 nm) (Figure 21). Moreover, the terminal nitrogen of the nitrile group was distant approximately 0.26 nm from the surface, thus the carbon in nitrile that mainly participates in the reaction was buried even deeper, resulting in very limited accessibility to this center, solely due to solvent structuring. Another important limitation originated from different approaches of reaction components to the surface that is made purely from the frontal side of GCN. This strict steric restriction could not be applied in any aliphatic structure that is otherwise free to rotate.

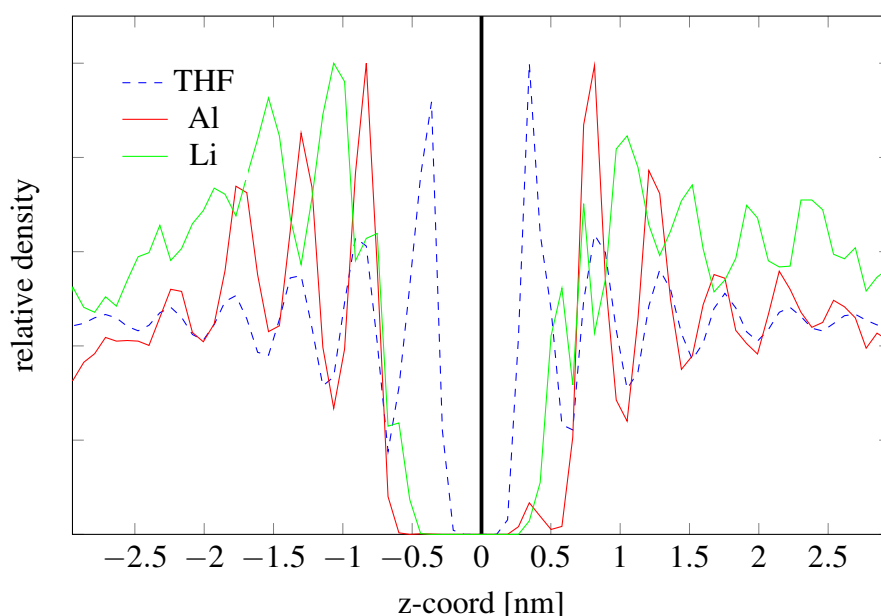


Figure 21: Relative density of solvent and LiAlH_4 along the z direction of the box. Black line symbolize graphene in the simulation box.

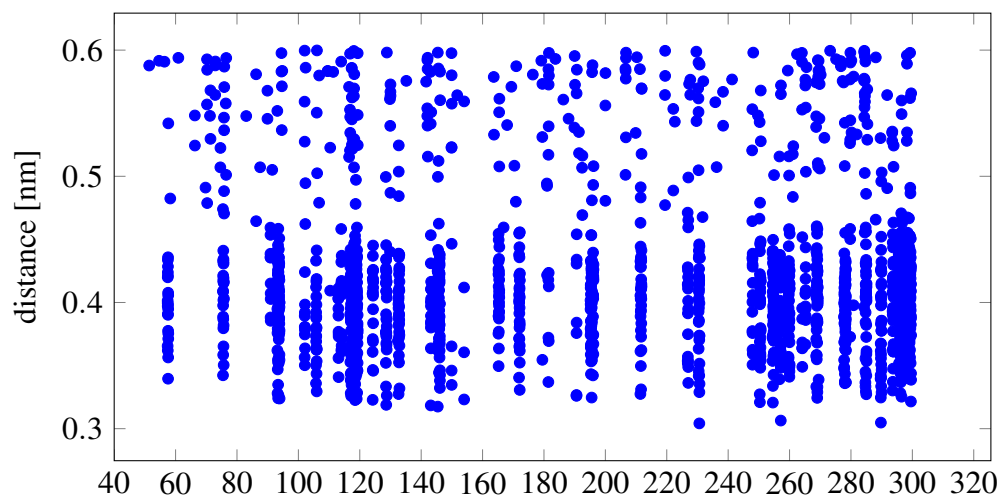
To gain deeper insight into the behavior of the reducing agent around the aliphatic nitriles and GCN, the residence time of the aluminum hydride in the vicinity of the nitrile group was analyzed. Table 2 shows an average time and mean distance between Al and N atoms when $[\text{AlH}_4]^-$ resided in the proximity of the nitrile group (only instances when hydride was closer than 0.5 nm were considered). Both observed quantities surprisingly provided very similar values regardless of the length of the aliphatic chain.

Table 2: Average lifetime and mean distance of $[\text{AlH}_4]^-$ around nitrile group.

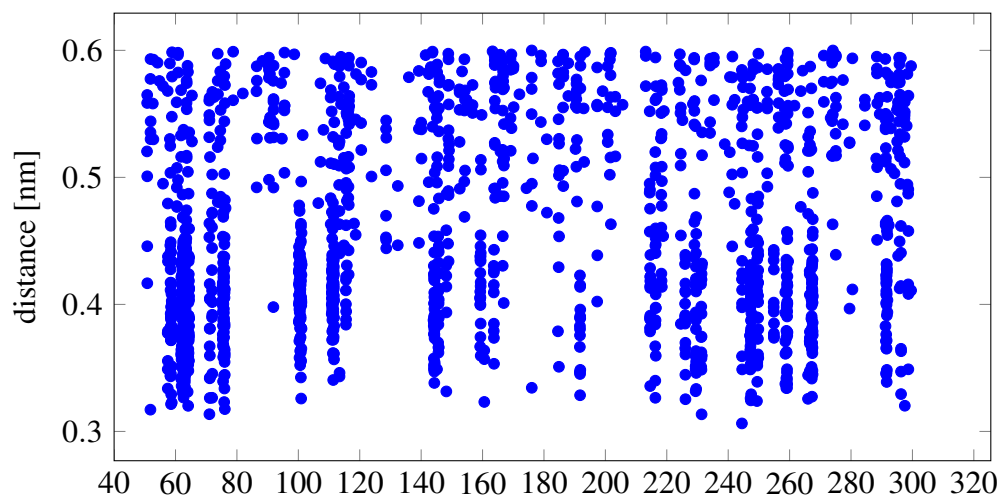
| System | Average residence time [ns] | Mean distance [nm] |
|----------|-----------------------------|--------------------|
| 1C | 0.18 ± 0.08 | 0.41 ± 0.05 |
| 4C | 0.20 ± 0.08 | 0.40 ± 0.03 |
| 5C | 0.20 ± 0.07 | 0.40 ± 0.04 |
| 6C | 0.15 ± 0.08 | 0.41 ± 0.04 |
| 7C | 0.17 ± 0.07 | 0.41 ± 0.04 |
| 8C | 0.18 ± 0.07 | 0.41 ± 0.04 |
| 9C | 0.20 ± 0.07 | 0.41 ± 0.04 |
| graphene | 0.26 ± 0.62 | 0.41 ± 0.03 |

It should be noted that in the case of GCN, the number of instances was very limited in our simulation time scale (300 ns), thus the average time is not suitable for direct comparison. However, the scattering plots (see Figure 22 for 4C, 6C, and graphene, and Figure S2 for the rest of the simulated molecules) showed clear differences in the number of instances for 4C, 6C, and GCN. 1C structure was in accord with already discussed RDFs, where the greatest accessibility for aluminum hydride was shown. In addition, when the aluminum hydride approached the nitrile closer than ≈ 0.45 nm, the connection was made resulting in the formation of an analogical initial state before the reduction reaction.

4C



6C



GCN

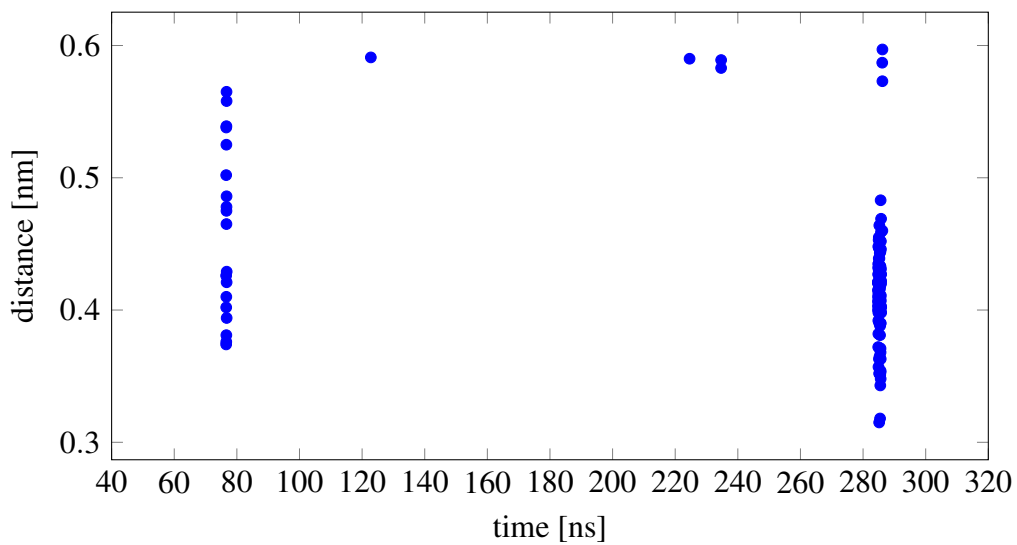


Figure 22: Scattering plots of distances between nitrogen from nitrile group in 4C, 6C and GCN and Al in LiAlH_4 .

As discussed above, single species participating in the reaction had to be aligned accurately prior to the reduction process. To identify the exact mutual orientation angles between C-N-Li and N-Li-Al, and torsion angle between all four atoms C-N-Li-Al was measured (for 4C, 6C and graphene molecules see Figure 24, and for rest of the molecules see Figure S3). Similarly as before, only samples with the distance between Al...CN closer than 0.5 nm were considered.

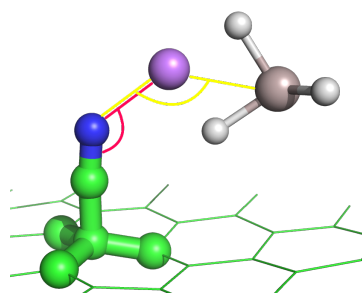


Figure 23: Measured angles.

Corresponding histograms showed that in the 6C system two dominant orientations of participating atoms were observed with a strong in-plane alignment. In the case of the shorter 4C chain only one structure without proper alignment was available (noticeably wider dihedral angle distribution ranging between -50° and 50°). The branched structure did not allow unimpeded access of the reducing agent from the bottom of the nitrile group. Obviously, this behaviour was even more pronounced in GCN with the accessibility being dominantly hampered by the highly ordered solvent as discussed above. On the contrary, 6C displayed the least steric interference between LiAlH_4 and the functional group and thus the reduction molecule could access the reaction state easily.

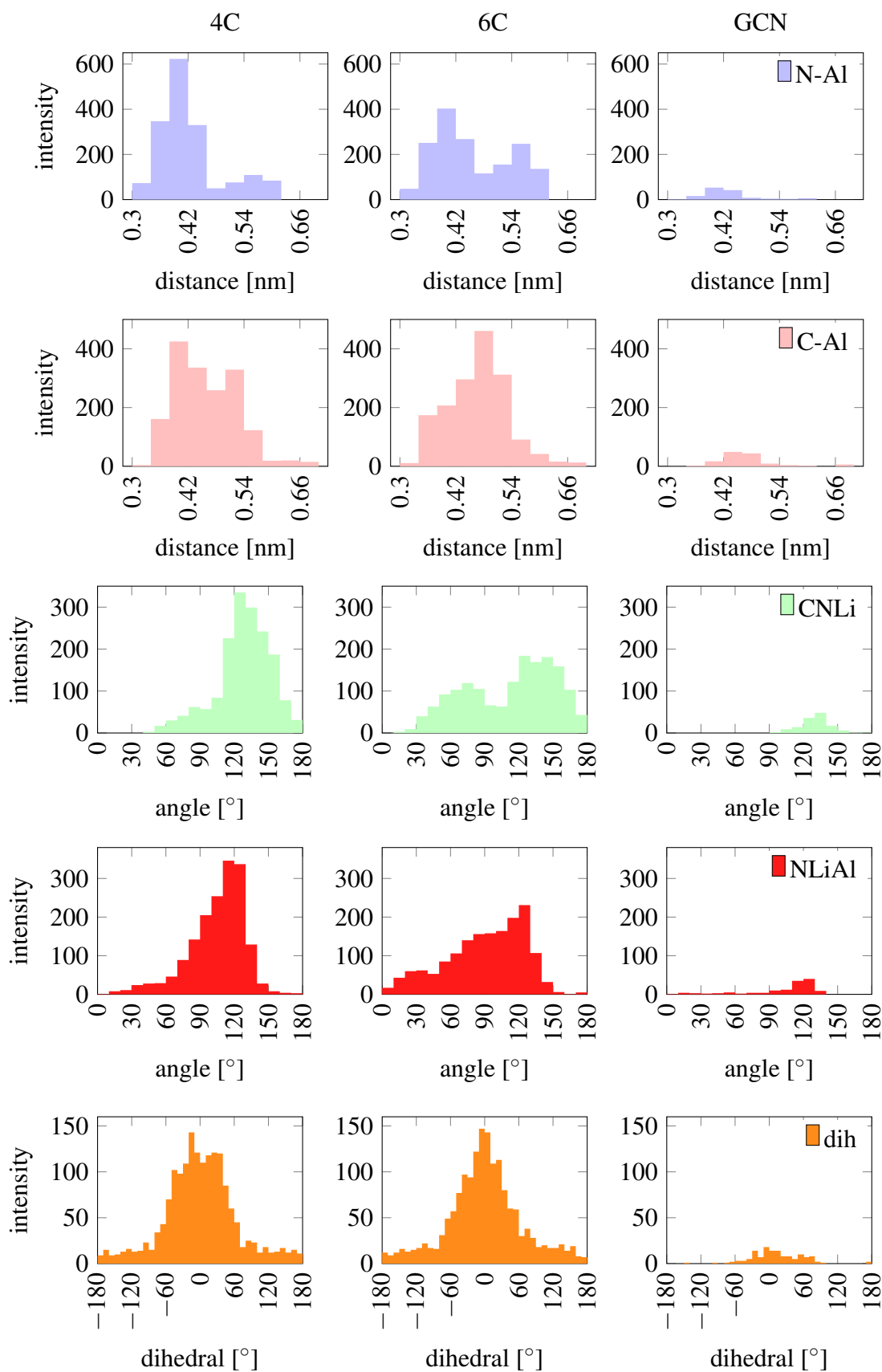


Figure 24: Histograms showing the distances between nitrogen (blue) or carbon (light red) of the nitrile group and aluminum, angles C-N-Li (green), N-Li-Al (red) and dihedral angle C-N-Li-Al (orange).

4.4.1 Access directions

Previous results indicated different approaches depending on the size of the system. Therefore, the movement vector of aluminum from the last 100 ns of the simulation was displayed with PyMOL software. [120] Each arrow represents the vector of the aluminum movement between two frames. Together with arrows are pictured average conformations of nitrile molecules (every 100th simulation frame). Moreover, I calculated also the electrostatic potential of molecules on B3LYP/6-31G* level using Gaussian G09 software [121] for better estimation of the field around molecule that may be responsible for the different accessibility.

For the shortest organic nitrile (acetonitrile), the aluminum hydride acceded the nitrile group from the methylated side of the molecule. The reason for this behavior can be explained by the positive potential on the methyl group that can attract the hydride anion from the reducing agent. This behavior is in agreement with RDF integrals above, where RDF of C was larger than in the case of N. In the 4C system, the direct approach (the hydride approached the nitrile group dominantly from the exposed side) towards the nitrile group was observed. Here the spacious *tert*-butyl group served as an effective repulsive shield for repelling molecules from its side. An alike mechanism was also preferred in the 5C system; however, the strict boundary was not as evident as in the 4C and still, the path from the aliphatic part of the molecule was sparsely populated.

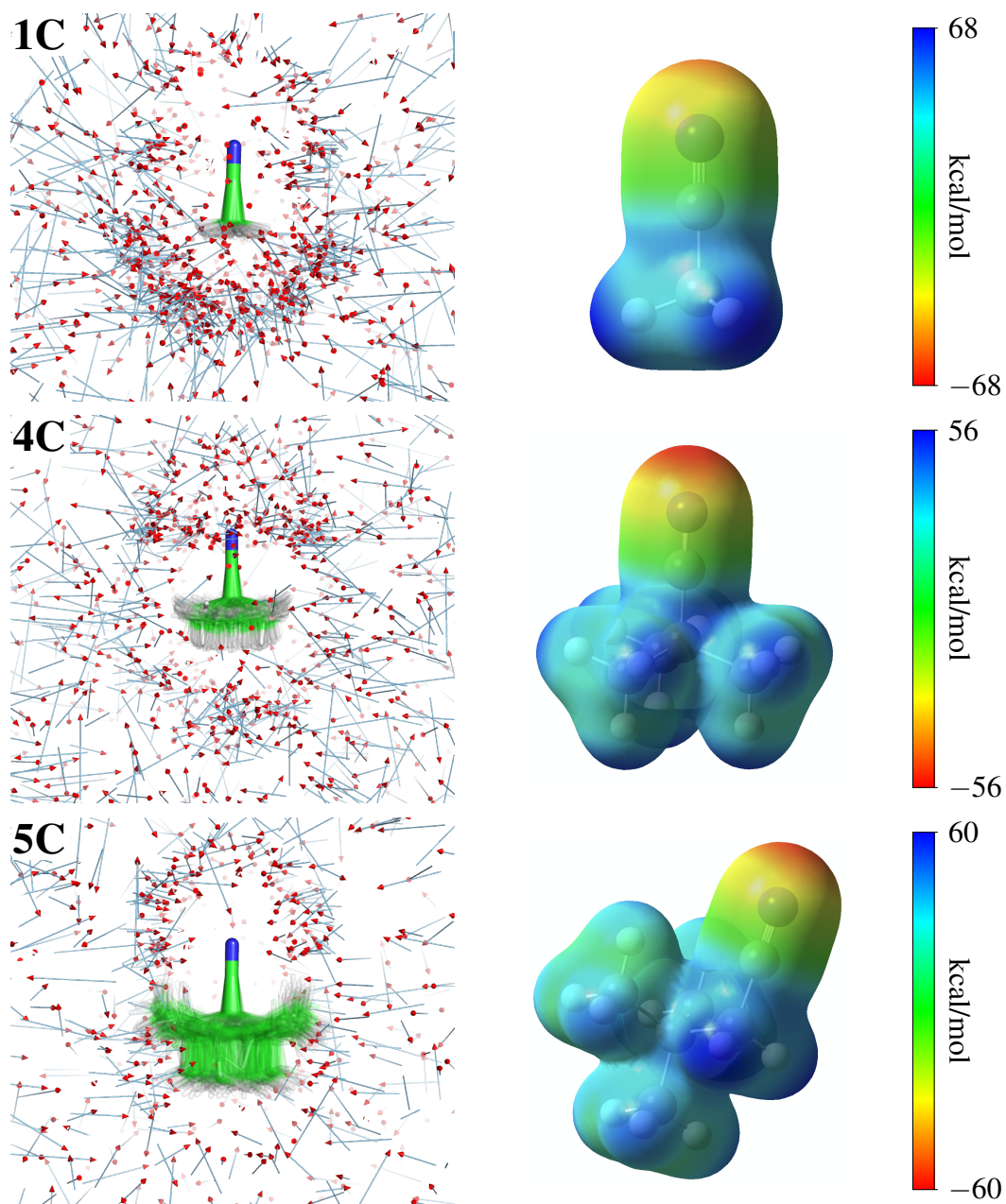


Figure 25: Nitrile group accessibility and corresponding ESP of studied systems with shorter aliphatic chain (1C, 4C and 5C). In the case of 1C the main access path was from methylated side, in of 4C and 5C LiAlH_4 accessed nitrile group directly.

In molecules with a longer aliphatic chain (6C, 7C, 8C, and 9C) the hydride anion approached almost predominantly from the aliphatic side of molecules. Similarly to 1C molecule, it may originate from the electrostatic potential generated by the molecule, where the positive potential around the α -carbon may attract the hydride anion and thus largely determine the accessibility.

In addition, examination of average structures showed that the chains with even number of carbons (here, the 8C) were prone to fill the free space around the nitrile and therefore decreasing the resulting group accessibility as was also observed in RDF. This can be seen in Figure 26, where terminal *tert*-butyl group got near to the functional groups, and disrupted reaction state of the functional group and the reducing agent. This behavior of the aliphatic chain was observed only in the system with 8C molecule.

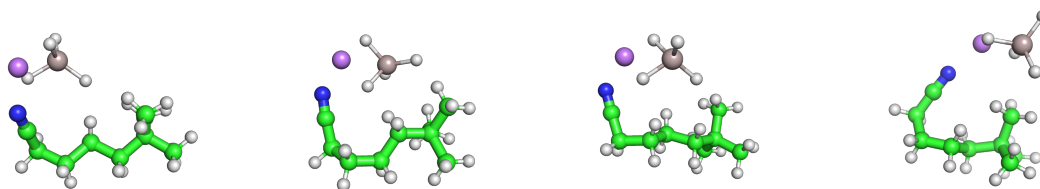


Figure 26: Interaction of terminal carbons with LiAlH_4 during the formation of the reactive state. Terminal *tert*-butyl group disrupted the formation of the reaction state between LiAlH_4 and nitrile group.

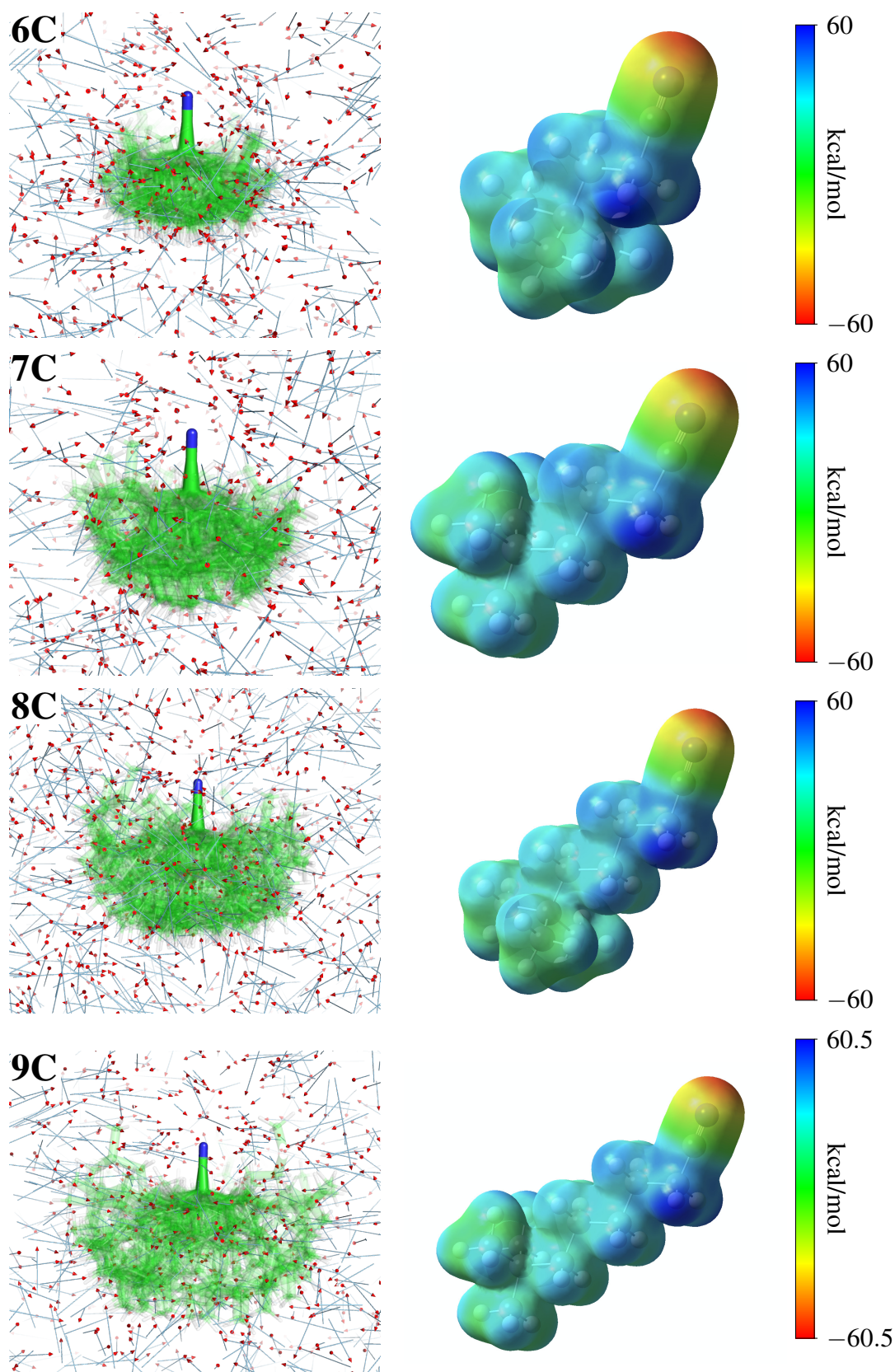


Figure 27: Nitrile group accessibility and corresponding ESP of studied systems with longer aliphatic chain (6C, 7C, 8C and 9C). The electrostatic potential shows positive potential under the nitrile group on α -C, which probably direct access of LiAlH_4 to nitrile group.

In the case of GCN, minimum aluminum hydrides were located near the surface. Moreover, the majority of the molecules were moved parallelly to the surface on the first solvent layer, which only supported the previously observed apparent barrier created by the solvent molecules. With that in mind, one can assume that the reduction of nitrile groups on GCN will not proceed very easily compared to other studied systems. It should be noted that the real experimental conditions may be affected by the fact that GCN may contain residual moisture that creates together with the reducing agent a local strong basic environment facilitating the final reduction process, such as in the case of GO as was described early. [87]

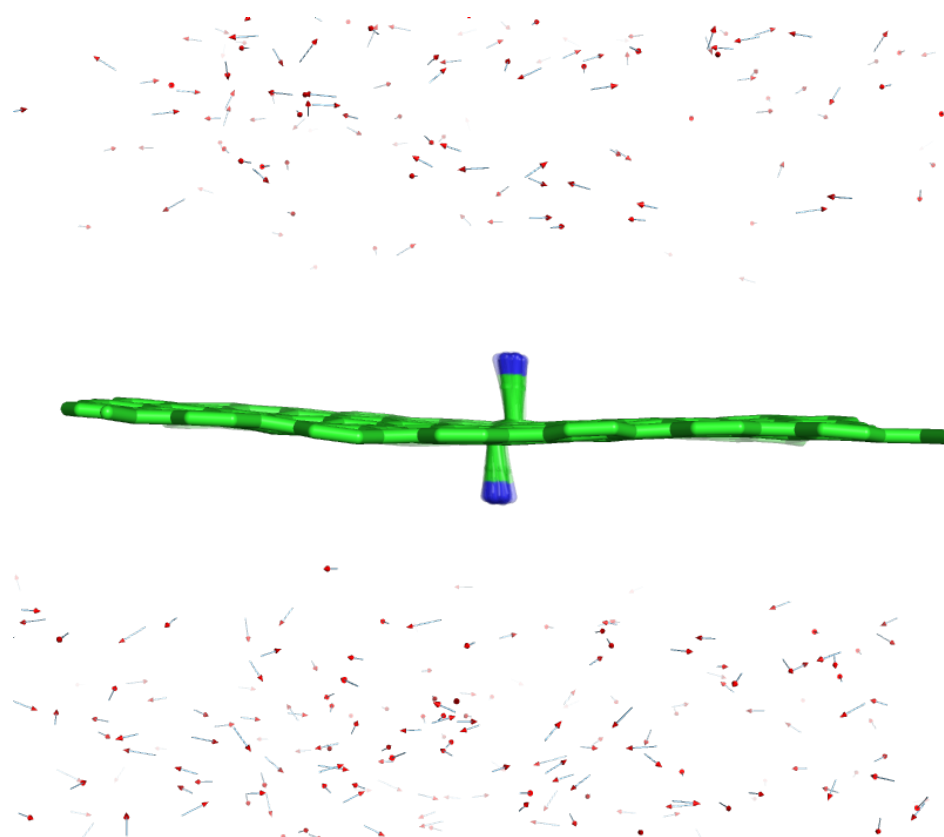


Figure 28: Nitrile group accessibility of GCN.

5. Summary

The goal of this thesis was to investigate the mechanistic part of the cyanographene reduction by LiAlH_4 . Utilizing classical molecular dynamics simulations allowed me to study the accessibility of the reducing agent to the nitrile group grafted on the graphene surface and compare it with aliphatic nitrile molecules.

First, I analyzed the effect of different solvents on the reduction of nitriles. This comparison showed that more polar solvents (DMF and water) are not suitable for the reduction of the nitrile group by LiAlH_4 , and the only system with THF displayed increased occurrence of LiAlH_4 in the vicinity of the nitrile group.

Further analysis of THF around the graphene surface revealed distinct layers of the solvent around graphene, which created a barrier for the LiAlH_4 molecule. The reducing agent resided mainly above the first layer. This indicated that strict THF layering hampered the accessibility to grafted groups located deep in the first solvent layer.

Moreover, analysis of aliphatic nitrile molecules showed different access directions based on the topology of the aliphatic chain. More sterically hindered nitrile groups displayed a direct approach of the reducing agent, where LiAlH_4 came to the functional group directly from the bulk. On the other hand, longer aliphatic nitrile molecules propagated access to the reducing agent from the aliphatic part of the molecule, probably caused by the positive electrostatic potential on α -carbon below the nitrile group.

The fact that the main access direction of LiAlH_4 to nitrile groups in aliphatic nitriles was directed by the electrostatic potential on α -carbon further discriminates GCN. This analysis of the access direction of LiAlH_4 together with its inability to properly breach the THF barrier can explain why the reduction of cyanographene has not been successfully carried out. However, the reduction mechanism of 2D materials is not a closed chapter, and further extensive studies are needed.

6. Závěr

Cílem této práce bylo prozkoumat mechanickou část redukce kyanografenu redukčním činidlem LiAlH_4 . Za tímto účelem jsem využíval metod molekulové mechaniky, pomocí kterých jsem analyzoval přístupnost redukujícího činidla k nitrilovým skupinám na alifatických molekulách a kyanografenu.

Jako první jsem porovnal vliv rozpouštědla na zkoumanou reakci. Srovnáním vody, DMF a THF jsem objevil, že pro úspěšný přístup molekuly LiAlH_4 k funkční skupině je vhodné pouze nepolární THF, zatímco LiAlH_4 v polárních rozpouštědlech neměl zvýšený výskyt v blízkosti nitrilové skupiny.

Následně jsem zkoumal interakci mezi nefunkcionalizovaným grafenem a THF. Obdobně jako je v literatuře popsáno pro další rozpouštědla, tak i THF tvoří několik vrstev na povrchu grafenu. V simulacích, kdy jsem zkoumal přímo přístupnost nitrilové skupiny se ukázalo, že LiAlH_4 se zdržoval převážně v druhé vrstvě. Fakt, že dusík v nitrilové skupině se nachází v první vrstvě THF ukazuje, že solvent tvoří překážku pro úspěšnou srážku nitrilové skupiny kyanografenu a LiAlH_4 .

Analýza přístupu dále ukázala, že v případě alifatických nitrilů se přístup LiAlH_4 liší v závislosti na topologii alifatického řetězce. Ke stéricky náročným nitrilům redukující činidlo přistupovalo přímo, zatímco u delších řetězců α -uhlík vytvářel kladný elektrostatický potenciál, který směřoval přístup LiAlH_4 k funkční skupině z alifatické části molekuly.

Souhrnně simulace ukázaly, že přístup LiAlH_4 k nitrilové skupině je ovlivněn dvěma nezávislými příspěvky - elektrostatickou přitažlivostí a entropickou repulzí alifatické části molekuly, popřípadě stérickou náročností 2D povrchu kyanografenu. Tento demonstrováný přístup LiAlH_4 k nitrilové skupině dále napovídá o znesnadnění přístupu LiAlH_4 k funkční skupině na povrchu grafenu, kdy je tento směr znemožněn. Toto srovnání společně s faktem, že redukujícímu činidlu znesnadňuje přístup vrstva THF může vysvětlovat, proč redukce kyanografenu stále nebyla úspěšně provedena. Na druhou stranu, chemie 2D materiálů není stále plně probádané téma a další studium této problematiky je bezpochyby potřeba.

Bibliography

- [1] V. Georgakilas, J. A. Perman, J. Tuček, and R. Zbořil. Broad family of carbon nanoallotropes: Classification, chemistry, and applications of fullerenes, carbon dots, nanotubes, graphene, nanodiamonds, and combined superstructures. *Chemical Reviews*, 115(11):4744–4822, 2015.
- [2] K. S. Novoselov, A. K. Geim, S. V. Morozov, D. Jiang, Y. Zhang, S. V. Dubonos, I. V. Grigorieva, and A. A. Firsov. Electric field effect in atomically thin carbon films. *Science*, 306(5696):666–669, 2004.
- [3] R. E. Peierls. Quelques propriétés typiques des corps solides. *Annales de l'Institut Henri Poincaré*, 5:177–222, 1934.
- [4] J. C. Meyer, A. K. Geim, M. I. Katsnelson, K. S. Novoselov, T. J. Booth, and S. Roth. The structure of suspended graphene sheets. *Nature*, 446(7131):60–63, 2007.
- [5] P. Miró, M. Audiffred, and T. Heine. An atlas of two-dimensional materials. *Chemical Society Reviews*, 43(18):6537–6554, 2014.
- [6] A. H. Castro Neto, F. Guinea, N. M. R. Peres, K. S. Novoselov, and A. K. Geim. The electronic properties of graphene. *Reviews of Modern Physics*, 81:109–162, 2009.
- [7] C. Lee, X. Wei, J. W. Kysar, and J. Hone. Measurement of the elastic properties and intrinsic strength of monolayer graphene. *Science*, 321(5887):385–388, 2008.
- [8] P. Zhang, L. Ma, F. Fan, Z. Zeng, C. Peng, P. E. Loya, Z. Liu, Y. Gong, J. Zhang, X. Zhang, P. M. Ajayan, T. Zhu, and J. Lou. Fracture toughness of graphene. *Nature Communications*, 5(1):3782, 2014.
- [9] M. D. Stoller, S. Park, Y. Zhu, J. An, and R. S. Ruoff. Graphene-based ultracapacitors. *Nano Letters*, 8(10):3498–3502, 2008.
- [10] A. K. Geim and K. S. Novoselov. The rise of graphene. *Nature Materials*, 6(3):183–191, 2007.
- [11] V. Singh, D. Joung, L. Zhai, S. Das, S. I. Khondaker, and S. Seal. Graphene based

- materials: Past, present and future. *Progress in Materials Science*, 56(8):1178–1271, 2011.
- [12] K. S. Novoselov, A. K. Geim, S. V. Morozov, D. Jiang, M. I. Katsnelson, I. V. Grigorieva, S. V. Dubonos, and A. A. Firsov. Two-dimensional gas of massless Dirac fermions in graphene. *Nature*, 438(7065):197–200, 2005.
- [13] K. I. Bolotin, K. J. Sikes, Z. Jiang, M. Klima, G. Fudenberg, J. Hone, P. Kim, and H. L. Stormer. Ultrahigh electron mobility in suspended graphene. *Solid State Communications*, 146(9-10):351–355, 2008.
- [14] J. Chen, C. Jang, S. Xiao, M. Ishigami, and M. S. Fuhrer. Intrinsic and extrinsic performance limits of graphene devices on SiO₂. *Nature Nanotechnology*, 3(4):206–209, 2008.
- [15] A. A. Balandin, S. Ghosh, W. Bao, I. Calizo, D. Teweldebrhan, F. Miao, and C. N. Lau. Superior thermal conductivity of single-layer graphene. *Nano Letters*, 8(3):902–907, 2008.
- [16] J. H. Seol, I. Jo, A. L. Moore, L. Lindsay, Z. H. Aitken, M. T. Pettes, X. Li, Z. Yao, R. Huang, D. Broido, N. Mingo, R. S. Ruoff, and L. Shi. Two-dimensional phonon transport in supported graphene. *Science*, 328(5975):213–216, 2010.
- [17] W. Cai, A. L. Moore, Y. Zhu, X. Li, S. Chen, L. Shi, and R. S. Ruoff. Thermal transport in suspended and supported monolayer graphene grown by chemical vapor deposition. *Nano Letters*, 10(5):1645–1651, 2010.
- [18] A. A. Balandin. Thermal properties of graphene and nanostructured carbon materials. *Nature Materials*, 10(8):569–581, 2011.
- [19] R. R. Nair, P. Blake, A. N. Grigorenko, K. S. Novoselov, T. J. Booth, T. Stauber, N. M.R. Peres, and A. K. Geim. Fine structure constant defines visual transparency of graphene. *Science*, 320(5881):1308, 2008.
- [20] B. Partoens and F. M. Peeters. From graphene to graphite: Electronic structure around the k point. *Physical Review B*, 74:075404, 2006.
- [21] L. Grande, V. T. Chundi, D. Wei, C. Bower, P. Andrew, and T. Ryhänen. Graphene for energy harvesting/storage devices and printed electronics. *Particuology*, 10(1):1–8, 2012.

- [22] Y. Gao, Z. Yan, J. L. Gray, X. He, D. Wang, T. Chen, Q. Huang, Y. C. Li, H. Wang, S. H. Kim, T. E. Mallouk, and D. Wang. Polymer–inorganic solid–electrolyte interphase for stable lithium metal batteries under lean electrolyte conditions. *Nature Materials*, 18(4):384–389, 2019.
- [23] C. Liu, Z. Yu, D. Neff, A. Zhamu, and B. Z. Jang. Graphene-based supercapacitor with an ultrahigh energy density. *Nano Letters*, 10(12):4863–4868, 2010.
- [24] S. Ghosh, G. Sahoo, S. R. Polaki, N. G. Krishna, M. Kamruddin, and T. Mathews. Enhanced supercapacitance of activated vertical graphene nanosheets in hybrid electrolyte. *Journal of Applied Physics*, 122(21):214902, 2017.
- [25] P. Suvarnapaet and S. Pechprasarn. Graphene-based materials for biosensors: A review. *Sensors*, 17(10):2161, 2017.
- [26] F. Bonaccorso, Z. Sun, T. Hasan, and A. C. Ferrari. Graphene photonics and optoelectronics. *Nature Photonics*, 4(9):611–622, 2010.
- [27] Z. Zhang, A. Fraser, S. Ye, G. Merle, and J. Barralet. Top-down bottom-up graphene synthesis. *Nano Futures*, 3(4):42003, 2019.
- [28] A. K. Geim. Graphene: Status and prospects. *Science*, 324(5934):1530 – 1534, 2009.
- [29] Y. Lin, K. A Jenkins, A. Valdes-Garcia, J. P Small, D. B. Farmer, and P. Avouris. Operation of graphene transistors at gigahertz frequencies. *Nano Letters*, 9(1):422–426, 2009.
- [30] F. Schedin, A. K. Geim, S. V. Morozov, E. W. Hill, P. Blake, M. I. Katsnelson, and K. S. Novoselov. Detection of individual gas molecules adsorbed on graphene. *Nature Materials*, 6(9):652–655, 2007.
- [31] Y. Hernandez, V. Nicolosi, M. Lotya, F. M. Blighe, Z. Sun, S. De, I. T. McGovern, B. Holland, M. Byrne, Y. K. Gun’Ko, J. J. Boland, P. Niraj, G. Duesberg, S. Krishnamurthy, R. Goodhue, J. Hutchison, V. Scardaci, A. C. Ferrari, and J. N. Coleman. High-yield production of graphene by liquid-phase exfoliation of graphite. *Nature Nanotechnology*, 3(9):563–568, 2008.
- [32] A. B. Bourlinos, V. Georgakilas, R. Zbořil, T. A. Steriotis, and A. K. Stubos. Liquid-phase exfoliation of graphite towards solubilized graphenes. *Small*, 5(16):1841–1845, 2009.

- [33] K. S. Novoselov, V. I. Fal'ko, L. Colombo, P. R. Gellert, M. G. Schwab, and K. Kim. A roadmap for graphene. *Nature*, 490(7419):192–200, 2012.
- [34] H. C. Schniepp, J. Li, M. J. McAllister, H. Sai, M. Herrera-Alonso, D. H. Adamson, R. K. Prud'homme, R. Car, D. A. Saville, and I. A. Aksay. Functionalized single graphene sheets derived from splitting graphite oxide. *The Journal of Physical Chemistry B*, 110(17):8535–8539, 2006.
- [35] S. Stankovich, D. A. Dikin, R. D. Piner, K. A. Kohlhaas, A. Kleinhammes, Y. Jia, Y. Wu, S. T. Nguyen, and R. S. Ruoff. Synthesis of graphene-based nanosheets via chemical reduction of exfoliated graphite oxide. *Carbon*, 45(7):1558–1565, 2007.
- [36] H. Shin, K. K. Kim, A. Benayad, S. Yoon, H. K. Park, I. Jung, M. H. Jin, H. Jeong, J. M. Kim, J. Choi, and Y. H. Lee. Efficient reduction of graphite oxide by sodium borohydride and its effect on electrical conductance. *Advanced Functional Materials*, 19(12):1987–1992, 2009.
- [37] S. Pei and H. M. Cheng. The reduction of graphene oxide. *Carbon*, 50(9):3210–3228, 2012.
- [38] K. V. Emtsev, A. Bostwick, K. Horn, J. Jobst, G. L. Kellogg, L. Ley, J. L. McChesney, T. Ohta, S. A. Reshanov, J. Röhrl, E. Rotenberg, A. K. Schmid, D. Waldmann, H. B. Weber, and T. Seyller. Towards wafer-size graphene layers by atmospheric pressure graphitization of silicon carbide. *Nature Materials*, 8(3):203–207, 2009.
- [39] I. Shteplyuk, V. Khranovskyy, and R. Yakimova. Combining graphene with silicon carbide: synthesis and properties – a review. *Semiconductor Science and Technology*, 31(11):113004, 2016.
- [40] J. Plutnar, M. Pumera, and Z. Sofer. The chemistry of CVD graphene. *Journal of Materials Chemistry C*, 6(23):6082–6101, 2018.
- [41] H. Y. Mao, S. Laurent, W. Chen, O. Akhavan, M. Imani, A. A. Ashkarran, and M. Mahmoudi. Graphene: Promises, facts, opportunities, and challenges in nanomedicine. *Chemical Reviews*, 113(5):3407–3424, 2013.
- [42] A. Narita, X. Wang, X. Feng, and K. Müllen. New advances in nanographene chemistry. *Chemical Society Reviews*, 44(18):6616–6643, 2015.
- [43] X. Wang, A. Narita, and K. Müllen. Precision synthesis versus bulk-scale fabrication

- of graphenes. *Nature Reviews Chemistry*, 2(1):100, 2017.
- [44] A. Eftekhari and H. Garcia. The necessity of structural irregularities for the chemical applications of graphene. *Materials Today Chemistry*, 4:1–16, 2017.
- [45] M. A. Bissett, S. Konabe, S. Okada, M. Tsuji, and H. Ago. Enhanced chemical reactivity of graphene induced by mechanical strain. *ACS Nano*, 7(11):10335–10343, 2013.
- [46] K. Tadyszak, J. K. Wychowanec, and J. Litowczenko. Biomedical applications of graphene-based structures. *Nanomaterials*, 8(11), 2018.
- [47] H. L. Poh, P. Šimek, Z. Sofer, I. Tomandl, and M. Pumera. Boron and nitrogen doping of graphene via thermal exfoliation of graphite oxide in a BF₃ or NH₃ atmosphere: contrasting properties. *Journal of Materials Chemistry A*, 1(42):13146–13153, 2013.
- [48] H. L. Poh, P. Šimek, Z. Sofer, and M. Pumera. Sulfur-doped graphene via thermal exfoliation of graphite oxide in H₂S, SO₂, or CS₂ gas. *ACS Nano*, 7(6):5262–5272, 2013.
- [49] L. Wang, Z. Sofer, and M. Pumera. Will any crap we put into graphene increase its electrocatalytic effect? *ACS Nano*, 14(1):21–25, 2020.
- [50] M. Pumera and C. H. A. Wong. Graphane and hydrogenated graphene. *Chemical Society Reviews*, 42:5987–5995, 2013.
- [51] D. C. Elias, R. R. Nair, T. M. G. Mohiuddin, S. V. Morozov, P. Blake, M. P. Halsall, A. C. Ferrari, D. W. Boukhvalov, M. I. Katsnelson, A. K. Geim, and K. S. Novoselov. Control of graphene's properties by reversible hydrogenation: Evidence for graphane. *Science*, 323(5914):610 LP – 613, 2009.
- [52] R. A. Schäfer, D. Dasler, U. Mundloch, F. Hauke, and A. Hirsch. Basic insights into tunable graphene hydrogenation. *Journal of the American Chemical Society*, 138(5):1647–1652, 2016.
- [53] D. R. Dreyer, S. Park, C. W. Bielawski, and R. S. Ruoff. The chemistry of graphene oxide. *Chemical Society Reviews*, 39:228–240, 2010.
- [54] D. Chen, H. Feng, and J. Li. Graphene oxide: Preparation, functionalization, and electrochemical applications. *Chemical Reviews*, 112(11):6027–6053, 2012.

- [55] J. W. Suk, R. D. Piner, J. An, and R. S. Ruoff. Mechanical properties of monolayer graphene oxide. *ACS Nano*, 4(11):6557–6564, 2010.
- [56] A. T. Smith, A. M. LaChance, S. Zeng, B. Liu, and L. Sun. Synthesis, properties, and applications of graphene oxide/reduced graphene oxide and their nanocomposites. *Nano Materials Science*, 1(1):31–47, 2019.
- [57] J. D. Renteria, S. Ramirez, H. Malekpour, B. Alonso, A. Centeno, A. Zurutuza, A. I. Cocemasov, D. L. Nika, and A. A. Balandin. Strongly anisotropic thermal conductivity of free-standing reduced graphene oxide films annealed at high temperature. *Advanced Functional Materials*, 25(29):4664–4672, 2015.
- [58] B. C. Brodie. XIII. On the atomic weight of graphite. *Philosophical Transactions of the Royal Society of London*, 149:249–259, 1859.
- [59] L. Staudenmaier. Verfahren zur Darstellung der Graphitsäure. *Berichte der deutschen chemischen Gesellschaft*, 31(2):1481–1487, 1898.
- [60] W. S. Hummers and R. E. Offeman. Preparation of graphitic oxide. *Journal of the American Chemical Society*, 80(6):1339, 1958.
- [61] A. M. Dimiev and J. M. Tour. Mechanism of graphene oxide formation. *ACS Nano*, 8(3):3060–3068, 2014.
- [62] S. Bano, A. Mahmood, S. Kim, and K. Lee. Graphene oxide modified polyamide nanofiltration membrane with improved flux and antifouling properties. *Journal of Materials Chemistry A*, 3(5):2065–2071, 2015.
- [63] J. Zhao, W. Ren, and H. Cheng. Graphene sponge for efficient and repeatable adsorption and desorption of water contaminations. *Journal of Materials Chemistry*, 22:20197–20202, 2012.
- [64] J. Xu, Z. Tan, W. Zeng, G. Chen, S. Wu, Y. Zhao, K. Ni, Z. Tao, M. Ikram, H. Ji, and Y. Zhu. A hierarchical carbon derived from sponge-templated activation of graphene oxide for high-performance supercapacitor electrodes. *Advanced Materials*, 28(26):5222–5228, 2016.
- [65] F. Kim, L. J. Cote, and J. Huang. Graphene oxide: surface activity and two-dimensional assembly. *Advanced Materials*, 22(17):1954–1958, 2010.

- [66] D. Pierleoni, M. Minelli, S. Ligi, M. Christian, S. Funke, N. Reineking, V. Morandi, F. Doghieri, and V. Palermo. Selective gas permeation in graphene oxide–polymer self-assembled multilayers. *ACS Applied Materials & Interfaces*, 10(13):11242–11250, 2018.
- [67] E. Aliyev, V. Filiz, M. M. Khan, Y. J. Lee, C. Abetz, and V. Abetz. Structural characterization of graphene oxide: surface functional groups and fractionated oxidative debris, 2019.
- [68] D. D. Chronopoulos, A. Bakandritsos, M. Pykal, R. Zbořil, and M. Otyepka. Chemistry, properties, and applications of fluorographene. *Applied Materials Today*, 9:60–70, 2017.
- [69] R. R. Nair, W. Ren, R. Jalil, I. Riaz, V. G. Kravets, L. Britnell, P. Blake, F. Schedin, A. S. Mayorov, S. Yuan, M. I. Katsnelson, H.-M. Cheng, W. Strupinski, L. G. Bulusheva, A. V. Okotrub, I. V. Grigorieva, A. N. Grigorenko, K. S. Novoselov, and A. K. Geim. Fluorographene: A two-dimensional counterpart of teflon. *Small*, 6(24):2877–2884, 2010.
- [70] F. Karlický and M. Otyepka. Band gaps and optical spectra of chlorographene, fluorographene and graphane from g0w0, gw0 and gw calculations on top of pbe and hse06 orbitals. *Journal of Chemical Theory and Computation*, 9(9):4155–4164, 2013.
- [71] R. Zbořil, F. Karlický, A. B. Bourlinos, T. A. Steriotis, A. K. Stubos, V. Georgakilas, K. Šafářová, D. Jančík, C. Trapalis, and M. Otyepka. Graphene fluoride: A stable stoichiometric graphene derivative and its chemical conversion to graphene. *Small*, 6(24):2885–2891, 2010.
- [72] A. B. Bourlinos, K. Safarova, K. Siskova, and R. Zbořil. The production of chemically converted graphenes from graphite fluoride. *Carbon*, 50(3):1425–1428, 2012.
- [73] H. Chang, J. Cheng, X. Liu, J. Gao, M. Li, J. Li, X. Tao, F. Ding, and Z. Zheng. Facile synthesis of wide-bandgap fluorinated graphene semiconductors. *Chemistry – A European Journal*, 17(32):8896–8903, 2011.
- [74] R. Stine, W.-K. Lee, K. E. Whitener, J. T. Robinson, and P. E. Sheehan. Chemical stability of graphene fluoride produced by exposure to XeF₂. *Nano Letters*, 13(9):4311–4316, 2013.

- [75] S.-H. Cheng, K. Zou, F. Okino, H. R. Gutierrez, A. Gupta, N. Shen, P. C. Eklund, J. O. Sofo, and J. Zhu. Reversible fluorination of graphene: Evidence of a two-dimensional wide bandgap semiconductor. *Physical Review B*, 81:205435, 2010.
- [76] V. Mazánek, O. Jankovský, J. Luxa, D. Sedmidubský, Z. Janoušek, F. Šembera, M. Mikulics, and Z. Sofer. Tuning of fluorine content in graphene: towards large-scale production of stoichiometric fluorographene. *Nanoscale*, 7:13646–13655, 2015.
- [77] V. Urbanová, F. Karlický, A. Matěj, F. Šembera, Z. Janoušek, J. A. Perman, V. Ranc, K. Čépe, J. Michl, M. Otyepka, and R. Zbořil. Fluorinated graphenes as advanced biosensors – effect of fluorine coverage on electron transfer properties and adsorption of biomolecules. *Nanoscale*, 8:12134–12142, 2016.
- [78] S. Das, P. Sudhagar, V. Verma, D. Song, E. Ito, S. Y. Lee, Y. S. Kang, and W. Choi. Amplifying charge-transfer characteristics of graphene for triiodide reduction in dye-sensitized solar cells. *Advanced Functional Materials*, 21(19):3729–3736, 2011.
- [79] A. Bakandritsos, M. Pykal, P. Błoński, P. Jakubec, D. D. Chronopoulos, K. Poláková, V. Georgakilas, K. Čépe, O. Tomanec, V. Ranc, A. B. Bourlinos, R. Zbořil, and M. Otyepka. Cyanographene and graphene acid: Emerging derivatives enabling high-yield and selective functionalization of graphene. *ACS Nano*, 11(3):2982–2991, 2017.
- [80] R. Langer, E. Fako, P. Błoński, M. Vavrečka, A. Bakandritsos, M. Otyepka, and N. López. Anchoring of single-platinum-adatoms on cyanographene: Experiment and theory. *Applied Materials Today*, 18:100462, 2020.
- [81] O. Jankovský, M. Nováček, J. Luxa, D. Sedmidubský, V. Fila, M. Pumera, and Z. Sofer. A new member of the graphene family: Graphene acid. *Chemistry – A European Journal*, 22(48):17416–17424, 2016.
- [82] A. Lenarda, A. Bakandritsos, M. Bevilacqua, C. Tavagnacco, M. Melchionna, A. Naldoni, T. Steklý, M. Otyepka, R. Zbořil, and P. Fornasiero. Selective functionalization blended with scaffold conductivity in graphene acid promotes H_2O_2 electrochemical sensing. *ACS Omega*, 4(22):19944–19952, 2019.
- [83] Y. H. Cheong, M. Z. M. Nasir, A. Bakandritsos, M. Pykal, P. Jakubec, R. Zbořil, M. Otyepka, and M. Pumera. Cyanographene and graphene acid: The functional group of graphene derivative determines the application in electrochemical sensing

- and capacitors. *ChemElectroChem*, 6(1):229–234, 2019.
- [84] R. Kumar, M. Kumar, A. Kumar, R. Singh, R. Kashyap, S. Rani, and D. Kumar. Surface modification of graphene oxide using esterification. *Materials Today: Proceedings*, 18:1556–1561, 2019.
- [85] N. Mohanty and V. Berry. Graphene-based single-bacterium resolution biodevice and dna transistor: interfacing graphene derivatives with nanoscale and microscale bio-components. *Nano Letters*, 8(12):4469–4476, 2008.
- [86] S. Wang, P. Chia, L. Chua, L. Zhao, R. Png, S. Sivaramakrishnan, M. Zhou, R. G.-S. Goh, R. H. Friend, A. T.-S. Wee, and P. K.-H. Ho. Band-like transport in surface-functionalized highly solution-processable graphene nanosheets. *Advanced Materials*, 20(18):3440–3446, 2008.
- [87] A. Ambrosi, C. K. Chua, A. Bonanni, and M. Pumera. Lithium aluminum hydride as reducing agent for chemically reduced graphene oxides. *Chemistry of Materials*, 24(12):2292–2298, 2012.
- [88] R. Salvio, S. Krabbenborg, W. J. M. Naber, A. H. Velders, D. N. Reinhoudt, and W. G. van der Wiel. The formation of large-area conducting graphene-like platelets. *Chemistry – A European Journal*, 15(33):8235–8240, 2009.
- [89] C. E. Halbig, P. Rietsch, and S. Eigler. Towards the synthesis of graphene azide from graphene oxide. *Molecules*, 20(12), 2015.
- [90] M. Medved', G. Zoppellaro, J. Ugolotti, D. Matochová, P. Lazar, T. Pospíšil, A. Bakandritsos, J. Tuček, R. Zbořil, and M. Otyepka. Reactivity of fluorographene is triggered by point defects: beyond the perfect 2D world. *Nanoscale*, 10(10):4696–4707, 2018.
- [91] R. Stine, J. W. Ciszek, D. E. Barlow, W.-K. Lee, J. T. Robinson, and P. E. Sheehan. High-density amine-terminated monolayers formed on fluorinated CVD-grown graphene. *Langmuir*, 28(21):7957–7961, 2012.
- [92] K. E. Whitener, R. Stine, J. T. Robinson, and P. E. Sheehan. Graphene as electrophile: Reactions of graphene fluoride. *The Journal of Physical Chemistry C*, 119(19):10507–10512, 2015.
- [93] V. Urbanová, K. Holá, A. B. Bourlinos, K. Čépe, A. Ambrosi, A. H. Loo, M. Pumera,

- F. Karlický, M. Otyepka, and R. Zbořil. Thiofluorographene–hydrophilic graphene derivative with semiconducting and genosensing properties. *Advanced Materials*, 27(14):2305–2310, 2015.
- [94] D. D. Chronopoulos, A. Bakandritsos, P. Lazar, M. Pykal, K. Čépe, R. Zbořil, and M. Otyepka. High-yield alkylation and arylation of graphene via grignard reaction with fluorographene. *Chemistry of Materials*, 29(3):926–930, 2017.
- [95] V. Mazánek, A. Libánská, J. Šturala, D. Bouša, D. Sedmidubský, M. Pumera, Z. Janoušek, J. Plutnar, and Z. Sofer. Fluorographene modified by grignard reagents: A broad range of functional nanomaterials. *Chemistry – A European Journal*, 23(8):1956–1964, 2017.
- [96] F. Huang, Y. Li, X. Liu, W. Lai, K. Fan, X. Liu, and X. Wang. Suzuki–Miyaura reaction of C–F bonds in fluorographene. *Chemical Communications*, 57(3):351–354, 2021.
- [97] P. Gong, J. Wang, W. Sun, D. Wu, Z. Wang, Z. Fan, H. Wang, X. Han, and S. Yang. Tunable photoluminescence and spectrum split from fluorinated to hydroxylated graphene. *Nanoscale*, 6(6):3316–3324, 2014.
- [98] V. Nguyen. Functionalization of graphene from electrochemical exfoliation and fluorographene reduction for use in polyurethane composite materials. Centria University of Applied Sciences, Kokkola, Finland, 2019. *Unpublished thesis*.
- [99] L. Piela. *Ideas of Quantum Chemistry*. Elsevier Science, 2 edition, 2014.
- [100] C. J. Cramer. *Essentials of Computational Chemistry: Theories and Models*. Wiley, 2 edition, 2004.
- [101] F. Jensen. *Introduction to Computational Chemistry*. Wiley, 2 edition, 2007.
- [102] A. R. Leach. *Molecular Modelling: Principles and Applications*. Pearson Education Limited, 2 edition, 2001.
- [103] P. E. M. Lopes, B. Roux, and A. D. MacKerell. Molecular modeling and dynamics studies with explicit inclusion of electronic polarizability: theory and applications. *Theoretical Chemistry Accounts*, 124(1):11–28, 2009.
- [104] W. D. Cornell, P. Cieplak, C. I. Bayly, and P. A. Kollman. Application of RESP

- charges to calculate conformational energies, hydrogen bond energies, and free energies of solvation. *Journal of the American Chemical Society*, 115(21):9620–9631, 1993.
- [105] M. Pykal, P. Jurečka, F. Karlický, and M. Otyepka. Modelling of graphene functionalization. *Physical Chemistry Chemical Physics*, 18:6351–6372, 2016.
- [106] R. W. Hockney, S. P. Goel, and J. W. Eastwood. Quiet high-resolution computer models of a plasma. *Journal of Computational Physics*, 14(2):148–158, 1974.
- [107] D. Van Der Spoel, E. Lindahl, B. Hess, G. Groenhof, A. E. Mark, and H. J. C. Berendsen. GROMACS: Fast, flexible, and free. *Journal of Computational Chemistry*, 26(16):1701–1718, 2005.
- [108] Chemistry of nitriles, (2021, March 16). Retrieved April 27, 2021, from <https://chem.libretexts.org/@go/page/36556>.
- [109] Y. Hori, T. Ida, and M. Mizuno. A comparative theoretical study of the hydride transfer mechanisms during LiAlH_4 and LiBH_4 reductions. *Computational and Theoretical Chemistry*, 1076:86–93, 2016.
- [110] W. D. Cornell, P. Cieplak, C. I. Bayly, I. R. Gould, K. M. Merz, D. M. Ferguson, D. C. Spellmeyer, T. Fox, James W. C., and P. A. Kollman. A second generation force field for the simulation of proteins, nucleic acids, and organic molecules. *Journal of the American Chemical Society*, 117(19):5179–5197, 1995.
- [111] A. Cheng and W. A. Steele. Computer simulation of ammonia on graphite. I. Low temperature structure of monolayer and bilayer films. *The Journal of Chemical Physics*, 92(6):3858–3866, 1990.
- [112] S. L. Mayo, B. D. Olafson, and W. A. Goddard. DREIDING: a generic force field for molecular simulations. *The Journal of Physical Chemistry*, 94(26):8897–8909, 1990.
- [113] Z. Yu, D. G. Mackanic, W. Michaels, M. Lee, A. Pei, D. Feng, Q. Zhang, Y. Tsao, C. V. Amanchukwu, X. Yan, H. Wang, S. Chen, K. Liu, J. Kang, J. Qin, Y. Cui, and Z. Bao. A dynamic, electrolyte-blocking, and single-ion-conductive network for stable lithium-metal anodes. *Joule*, 3(11):2761–2776, 2019.
- [114] H. J. C. Berendsen, J. R. Grigera, and T. P. Straatsma. The missing term in effective pair potentials. *The Journal of Physical Chemistry*, 91(24):6269–6271, 1987.

- [115] C. Caleman, P. J. van Maaren, M. Hong, J. S. Hub, L. T. Costa, and D. van der Spoel. Force Field Benchmark of Organic Liquids: Density, Enthalpy of Vaporization, Heat Capacities, Surface Tension, Isothermal Compressibility, Volumetric Expansion Coefficient, and Dielectric Constant. *Journal of Chemical Theory and Computation*, 8(1):61–74, 2012.
- [116] D. van der Spoel, P. J. van Maaren, and C. Caleman. GROMACS molecule & liquid database. *Bioinformatics*, 28(5):752–753, 2012.
- [117] D. E. Bikiel, F. Di Salvo, M. C. González Lebrero, F. Doctorovich, and D. A. Estrin. Solvation and structure of LiAlH_4 in ethereal solvents. *Inorganic Chemistry*, 44(15):5286–5292, 2005.
- [118] F. Goujon, A. Ghoufi, and P. Malfreyt. Associated molecular liquids at the graphene monolayer interface. *The Journal of Chemical Physics*, 154(10):104504, 2021.
- [119] D. Konatham and A. Striolo. Molecular Design of Stable Graphene Nanosheets Dispersions. *Nano Letters*, 8(12):4630–4641, 2008.
- [120] Schrödinger, LLC. The PyMOL molecular graphics system, version 1.8. 2015.
- [121] M. J. Frisch, G. W. Trucks, H. B. Schlegel, G. E. Scuseria, M. A. Robb, J. R. Cheeseman, G. Scalmani, V. Barone, B. Mennucci, G. A. Petersson, H. Nakatsuji, M. Caricato, X. Li, H. P. Hratchian, A. F. Izmaylov, J. Bloino, G. Zheng, J. L. Sonnenberg, M. Hada, M. Ehara, K. Toyota, R. Fukuda, J. Hasegawa, M. Ishida, T. Nakajima, Y. Honda, O. Kitao, H. Nakai, T. Vreven, J. A. Montgomery, J. E. Peralta, F. Ogliaro, M. Bearpark, J. J. Heyd, E. Brothers, K. N. Kudin, V. N. Staroverov, R. Kobayashi, J. Normand, K. Raghavachari, A. Rendell, J. C. Burant, S. S. Iyengar, J. Tomasi, M. Cossi, N. Rega, J. M. Millam, M. Klene, J. E. Knox, J. B. Cross, V. Bakken, C. Adamo, J. Jaramillo, R. Gomperts, R. E. Stratmann, O. Yazyev, A. J. Austin, R. Cammi, C. Pomelli, J. W. Ochterski, R. L. Martin, K. Morokuma, V. G. Zakrzewski, G. A. Voth, P. Salvador, J. J. Dannenberg, S. Dapprich, A. D. Daniels, Ö Farkas, J. B. Foresman, J. V. Ortiz, J. Cioslowski, and D. J. Fox. Gaussian 09 Revision A.2. Wallingford, CT, 2009.

Supplementary Material

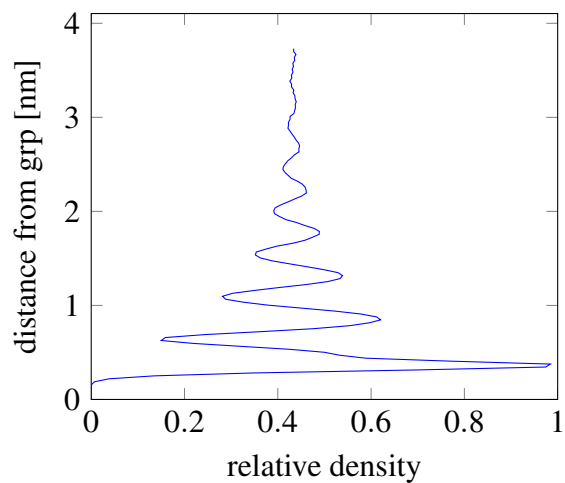


Figure S1: Relative density of THF above graphene.

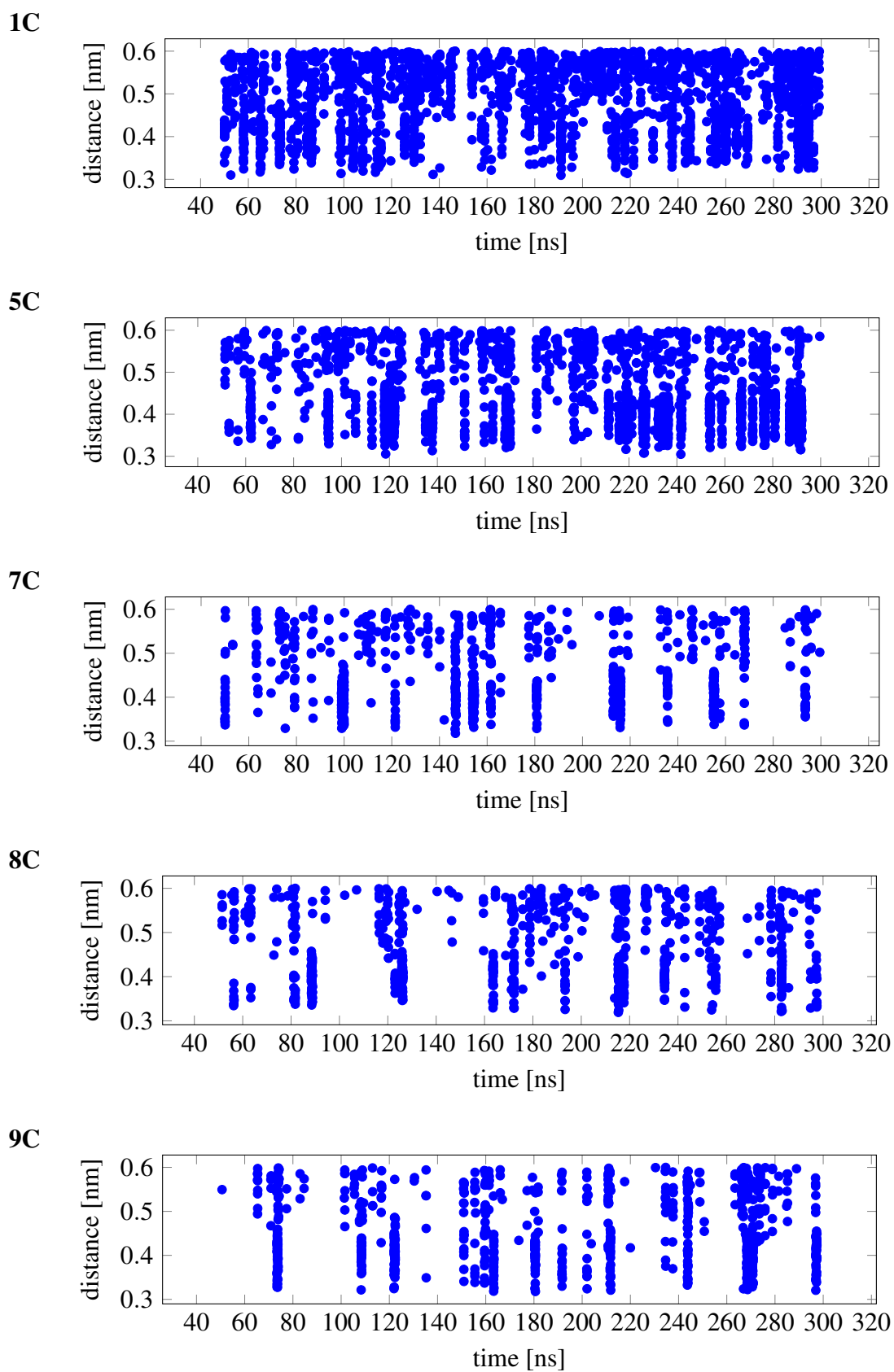


Figure S2: Scattering plots of distances between nitrogen from CN group in 1C, 5C, 7C, 8C and 9C and Al in LiAlH_4 .

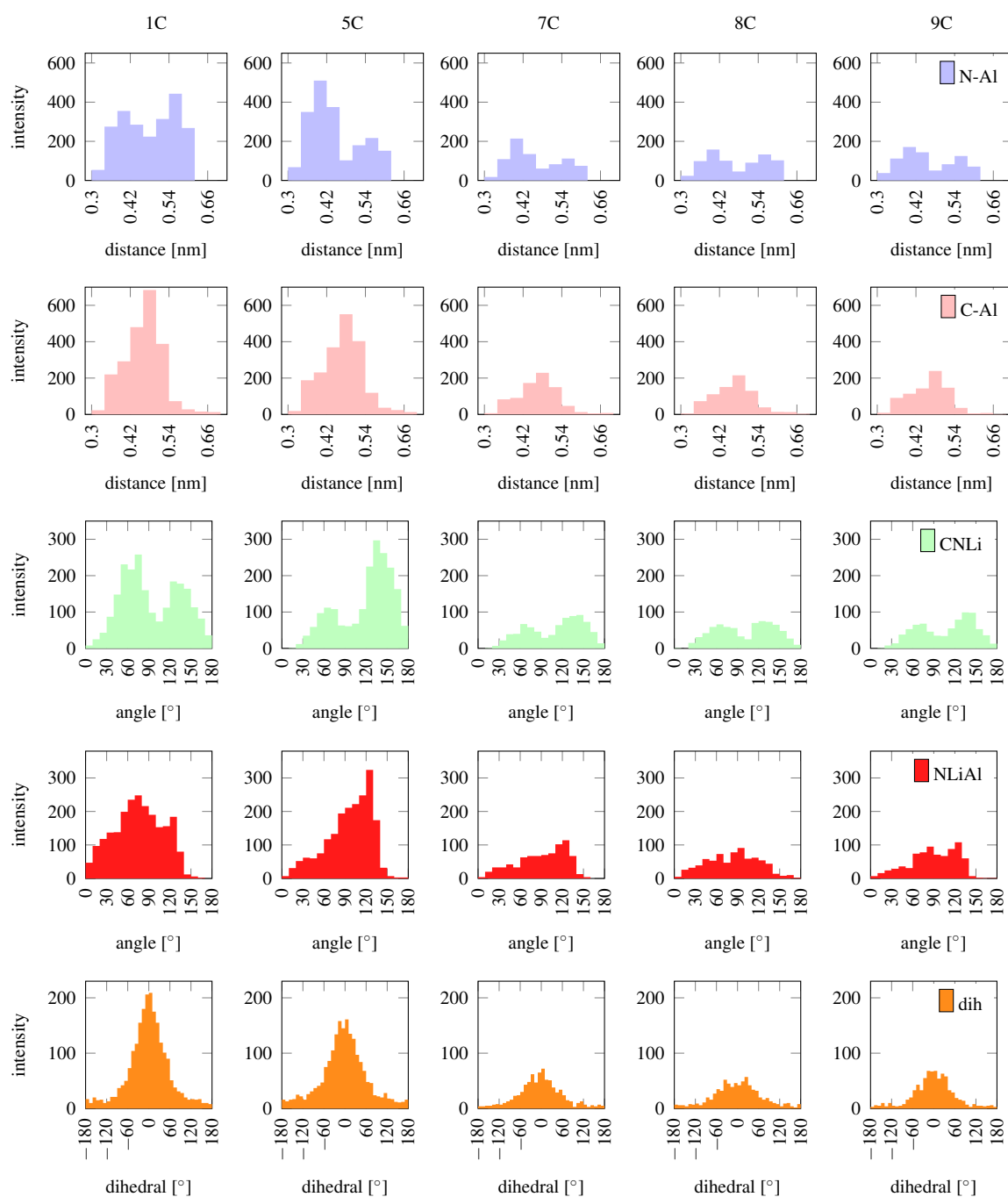


Figure S3: Histograms showing the distances between nitrogen (blue) or carbon (light red) of the CN group and aluminum, angles C-N-Li (green), N-Li-Al (red) and dihedral angle C-N-Li-Al (orange).